THE INFLUENCE OF CALCIUM INFILTRATION ON THE SINTERING BEHAVIOR AND DISSOLUTION OF BETA-TRICALCIUM PHOSPHATE

by

Yiwen Wei

B.S. in Materials Science and Engineering, University of Science and Technology Beijing, 2013

Submitted to the Graduate Faculty of

Swanson School of Engineering in partial fulfillment

of the requirements for the degree of

Master of Science in Materials Science and Engineering

University of Pittsburgh

2015

UNIVERSITY OF PITTSBURGH

SWANSON SCHOOL OF ENGINEERING

This thesis was presented

by

Yiwen Wei

It was defended on

April 1, 2015

and approved by

Ian Nettleship, PhD, Associate Professor, Department of Mechanical Engineering and Materials Science

Jung-kun Lee, PhD, Associate Professor, Department of Mechanical Engineering and Materials Science

Markus Chmielus, PhD, Assistant Professor, Department of Mechanical Engineering and Materials Science

Thesis Advisor: Ian Nettleship, PhD, Associate Professor, Department of Mechanical Engineering and Materials Science

THE INFLUENCE OF CALCIUM INFILTRATION ON THE SINTERING BEHAVIOR AND DISSOLUTION OF BETA-TRICALCIUM PHOSPHATE

Yiwen Wei, M.S.

University of Pittsburgh, 2015

Beta-Tricalcium phosphate (β-TCP) has attracted attention as a scaffold material for bone tissue engineering. The calcium content in β-TCP is thought to have an important influence on the sintering and biodegradability of the scaffold and the growth of bone tissue. The aim of this thesis was to process a β-TCP scaffold with enhanced solubility by infiltration of porous TCP with a calcium salt. The sintering behavior and phase distribution of Ca infiltrated β-TCP was investigated using relative density measurement, SEM observation and XRD analysis. High temperature sintering was only able to achieve a relative density of 89% and showed evidence of liquid phase formation consistent calcium deficient β-TCP. The liquid phase formation is thought to have caused coarsening of the microstructure that limited the final density. Similar studies were also conducted on Ca-infiltrated β-TCP. The results suggest that Ca-infiltration results in the stabilization of α-TCP rather than the formation of significant amounts of other calcium rich phases, which is thought to enhance degradation when the materials were immersed in water. Additionally, β-TCP foam was successfully processed using an emulsion based direct foaming method. Immersion of the foams in water showed no evidence of the enhanced degradation due to calcium rich phases.

TABLE OF CONTENTS

LIST OF TABLES

LIST OF FIGURES

1.0 INTRODUCTION

Regenerative medicine of bone and bone marrow has developed fast over decades, from pioneering achievement with bone marrow transplants for select hematological disorders to the recent success in bioengineered stem cell platforms.[1] The bone marrow transplantation includes both whole bone marrow cell transplantation and hematopoietic stem cells transplantation (HSCT). HSCT was firstly introduced in 1950s, developed afterwards and has become the most effective treatment for leukemia.[2] According to survey conducted by Worldwide Network for Blood and Marrow Transplantation, 51,536 cases of hematopoietic stem cell transplantation have been performed in 72 countries worldwide.[3] Despite of this widely use of bone marrow cell transplantation, it is facing several difficult problems in clinical application. Allogeneic HSCT(stem cells come from a donor) can cause graft-versus-host disease because the white blood cells from the donor may attack the cells in the host body.[4] An alternative is autologous HSCT, which avoids the problems with allogeneic HSCT. However, this option is inhibited because of the difficulty in obtaining a large enough population of health hematopoietic stem cells from the patient, especially after they have been subject to a partial or complete bone marrow ablation.[5]

Tissue engineering, as a main approach for regenerative medicine, focuses on development of a functional substitute for damaged tissue by combining principles of biology and engineering. This field of study provides the a potential method of increasing the population

of bone marrow stem cells in an in-vitro environment before implanting into the host body, therefore avoiding the problems of autologous HSCT. Tissue engineering usually involves a substrate material, known as scaffold, whose function is providing a surface and void volume that improves the attachment, migration, proliferation and desired differentiation of stem cells and tissue progenitors.[6] Biocompatibility and biodegradability is highly preferred for such a scaffold. Two phases of calcium phosphate compounds are the most attractive scaffold materials for bone and bone marrow because of their excellent bioactivity and biocompatibility due to their similarity in structure and composition to the mineral phase of bone.[7] Hydroxyapatite (HA) has been studied widely as a scaffold material. However, the problem, of low biodegradability of HA impedes bone ingrowth and results in weak chemical bonding between bones and HA implant, thereby limiting the application of HA as a scaffold.[8] An alternative choice among calcium phosphates is β-tricalcium phosphate (β-TCP). It is regarded as a resorbable bioceramic with better biodegradability, but worse biocompatibility than HA.

This thesis is based on the hypothesis that Ca infiltration of porous calcium phosphates has the ability of improving the biodegradability of the scaffold, by introducing water-soluble phases. However this must be done with care, researches[9,10] have shown that very high Ca content can have a negative effect on the function and differentiation of the stem cells. So the main purpose of this dissertation is to produce a rapid biodegradable scaffold of β-TCP with enhanced calcium release by Ca infiltration without exceeding the accepted calcium limit for cell culture. The infiltration should result in high calcium concentration near the scaffold surface and thereby promote cell attachment.

The sintering behavior of β-TCP is complex, since it difficult to achieve full density in β-TCP and, α-TCP is expected to be formed above 1180°C according to the $CaO–P_2O_5$ phase

diagram. However, this temperature changes significantly with different Ca content. In this study the sintering behavior of β-TCP was investigated and it is concluded that higher ratio of Ca/P has a positive effect on stabilizing α-TCP but no significant amounts of calcium rich phases were detected in the Ca-infiltrated samples.

2.0 BACKGROUND

2.1 REGENERATIVE MEDICINE

Regenerative medicine is defined as the fast developing interdisciplinary field of clinical therapies on the reconstruction, repair, replacement or regeneration of missing or damaged cells, tissues or organs, to restore its native architecture or function. [11] From pioneering achievement with bone marrow transplants for select hematological disorders to the recent success in bioengineered stem cell platforms, regenerative medicine has developed rapidly over the last two decades.[12] Regenerative medicine is regarded as “long-term promising” field by NIH, National Institutes of Health, for its important role in modern medical practice.[13] Usually, a combination of several approaches is used in regenerative medicine, including the use of soluble molecules, cell therapy, gene therapy, tissue engineering, immunomodulation therapy, etc.[14]

2.1.1 Cell therapy

Usually regarded as a sub-class of regenerative medicine, cell therapy is defined as the administration of cellular materials or maturation of a specific cell population in a patient to treat a disease or to repair a damaged tissue.[15] Cell therapy is usually achieved by the transplanting isolated and characterized cells to a target organ with sufficient number and quality to survive long enough to restore its function.[16]Although the first type of cell therapy was blood

transfusion, which appears much earlier than modern cell therapy, the Swiss physician Paul Niehans, MD, is widely accepted as the inventor of cell therapy, for his successful treatment of a patient who had damaged parathyroid glands by injecting a solution containing ground-up parathyroid cells from a calf.[17]The practice of injecting animal cells into human as an attempt to cure disease is one branch of today's cell therapy. However it is mainstream, since it is mostly ineffective, dangerous and controversial.

Nowadays cell therapy focuses on human cells transplanted from a donor to a recipient. Since stem cells can now be isolated from a diverse range of human tissues they are promising part of cell therapy. Stem cells are capable of replenishing their own number and also differentiating into more than one cell type.[18] Based on the concept of immunotherapy, which is a treatment of disease by inducing, enhancing, or suppressing an immune response,[19] clinicians are utilizing stem cells for cell therapies that have successfully treated several diseases.[20] For instance, allogeneic bone marrow transplantation is the treatment of choice for many kinds of blood disorders, including anemias, leukemias, lymphomas, and rare immunodeficiency diseases.[21] Cell therapy is also being used in the treatment to Parkinson's diseases[22], ischemic cardiomyopathy[23], brain repair,[24] and cardiovascular repair,[25] etc.

Embryonic stem cell therapies are also being considered because of the ability of embryonic stem cells to differentiate into a wide range of cell types, but this is controversial because for the stem cell source and it is banned in many countries.

According to a recently investigation, the estimated annual revenue in cell therapy industry was $5.1 billion in 2014.[26] There is no doubt that cell therapies will continue to expand.

2.1.2 Tissue engineering

Tissue engineering, applies the principles of biology and engineering by combining cells, engineering principles, and materials method to the development of functional substitutes for damaged tissue.[27] These tissues including skin, liver, pancreas, kidney, bone, etc. have been demonstrated and applied in some clinical applications.[28] Unlike replacing the failing organs mechanically, or using synthetic replacements, engineered tissues minimizes the risk of infection and device rejection

Previously research in tissue engineering has used differentiated cells such as fibroblasts in skin replacement and chondrocytes in cartilage repair. With the progress in stem cell biology and the recognition of the unique biological properties of stem cells, tissue engineering using stem cells has become of great interest to researchers.[29] Tissue engineering also involves a substrate material, known as the scaffold, to assist the organization of the cells in three-dimension, before the cells, which have their tissue-specific function, is implanted to patients.[30] Furthermore, in-vitro 3D cell culturing in bioreactors will require a scaffold. Bioreactor will be needed for extensive culturing of the primary human cells needed to improve survival, growth and inducement of functionality of the engineered tissue. A bioreactor is an engineered device or system that supports a biologically active environment by controlling parameters including oxygen, pH, humidity, temperature, nutrients and osmotic pressure required for culturing.

Bone tissue engineering, is one of the leading areas in tissue engineering, due to the need to alleviate the demand for bone tissue arising from the shortage of suitable auto graft and allograft materials for augmenting bone healing.[31] However, few researchers have reported successfully engineer bone marrow tissue, the focus of this thesis. [32] The use of porous material scaffolds made from bioceramic and polymer components to support bone cell function and

tissue growth is a lasting area of interest. However, there are challenges in the engineering of materials that can match both the mechanical and biological demand of real bone tissue matrix and support the vascularization of large tissue constructs.[33]

2.2 BONE STRUCTURE

Bone is a hierarchically structured composite that has long held the attention of the materials engineers who seek to duplicate its mechanical properties.[34] The hierarchical organization of bone ranging from the components to the whole bone is summarized in figure 1. This section will introduce bone structure briefly.

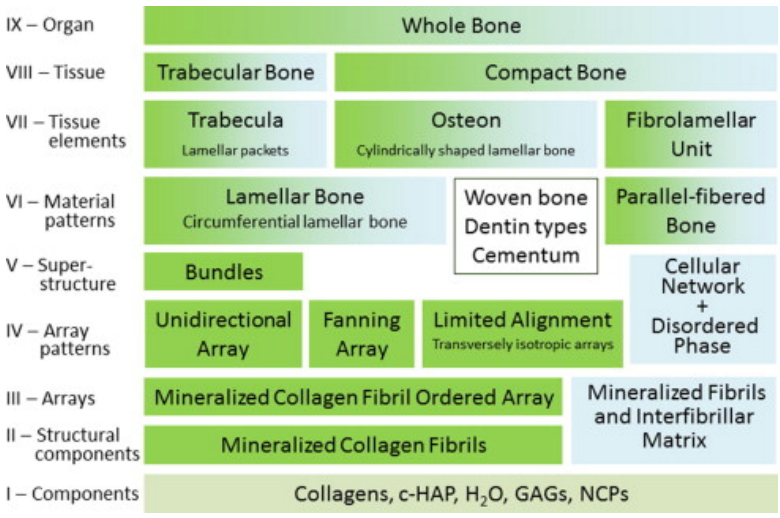

Figure 1: Hierarchical organization of bone[35]

At the molecular level, bone can be seen as a composite material composing of a fibrous protein, collagen, stiffened by a highly dense filling of calcium phosphate crystals. Other

components such as water, certain proteins and polysaccharides are also found in bone at the molecular level.

At the cellular level, various kinds of specialized cells exist in bone simultaneously. Bone-lining cells cover all surfaces of bones, constructing a thin continuous film that controls the movement of ions between the body and the bone. Osteoblasts derive from bone-lining cells and are responsible for the formation of bone. Osteocytes are the cells in the body of the bone. They derive from osteoblasts. They are imprisoned in the hard bone tissue and connect with neighboring osteocytes and with bone-lining cells by means of processes that occur in the little channels between the bone tissues. Osteoclasts are large, multinucleated cells derived from precursor cells circulating in the blood, and help dissolve bone during the constant restructuring that occurs in natural bone. When osteoclasts have done their job they die. [36]

At longer length scales there are two main types of bone architecture, cortical and trabecular bone which have distinct mechanical properties and mechanical functions. Bone marrow, is a very important tissue in bone, and will also be introduced below. Figure 2 shows the basic structures and tissues in common bone.

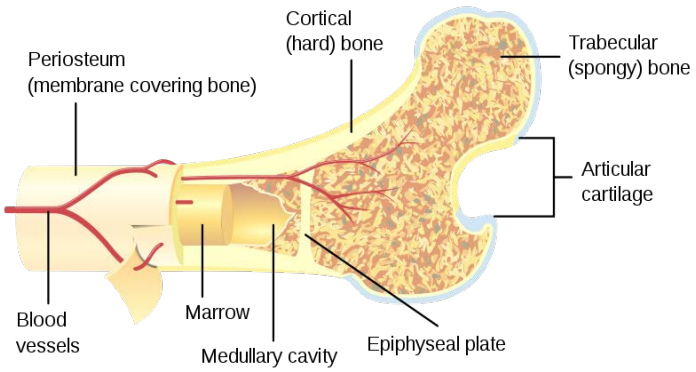

Figure 2: Schematic diagram for bone structure[37]

2.2.1 Cortical bone

Cortical bone, also synonymous with compact bone, is the hard outer layer of bone, which gives bone its smooth, white and solid surface, accounting for 80% of total bone mass in an adult[38,39] The basic unit of cortical bone, called an osteon, are arranged in columns with multiple layers of osteoblasts and osteocytes arranged around a central canal called the Haversian canal. Cortical bone is covered by a periosteum, a membrane layer between bones and skins,[40] on its outer surface, and an endosteum, which is a thin layer that lines the surface of the bone tissue, [40] on its inner surface. The endosteum is the boundary between the cortical bone and the trabecular bone.[41] Cortical bone facilitates bone's main functions of supporting the whole body, protecting organs, providing levers for movement, and administrating chemical elements, mainly calcium. Figure 3 schematically shows the position and structure of cortical bone (compact bone).

2.2.2 Trabecular bone

Trabecular bone, synonymous with cancellous bone or spongy bone is a porous network filling the interior of large bones. Trabecular bone accounts for the remaining 20% of total bone mass, but has nearly ten times the surface area of compact bone.[42] Trabecular bone has a much higher surface area to mass ratio compared to cortical bone, for it is less dense, giving it a softer but more flexible properties. The larger surface also enables trabecular bone to be a perfect bone type for metabolic activity, such as exchange of ions especially calcium. Typically, trabecular bone is found at the ends of long bones. Most importantly, it is highly vascular and frequently

contains red bone marrow, where blood cell produces hematopoiesis.[43] Figure 4 displays the bony trabeculae (pink) and marrow tissue (purple) in trabecular bone.

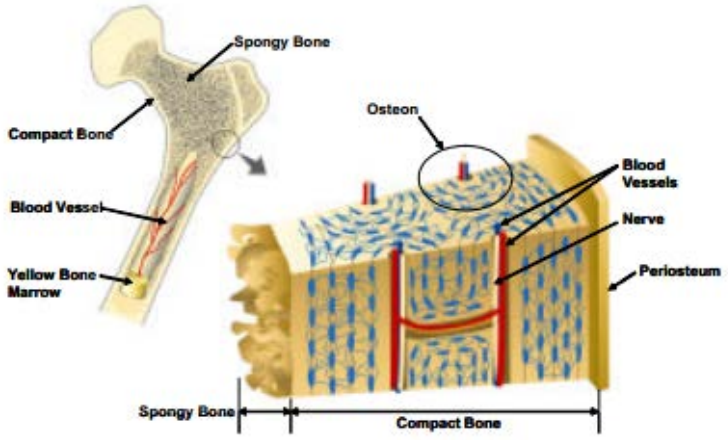

Figure 3: Hierarchical structure of human cortical (compact bone) [44]

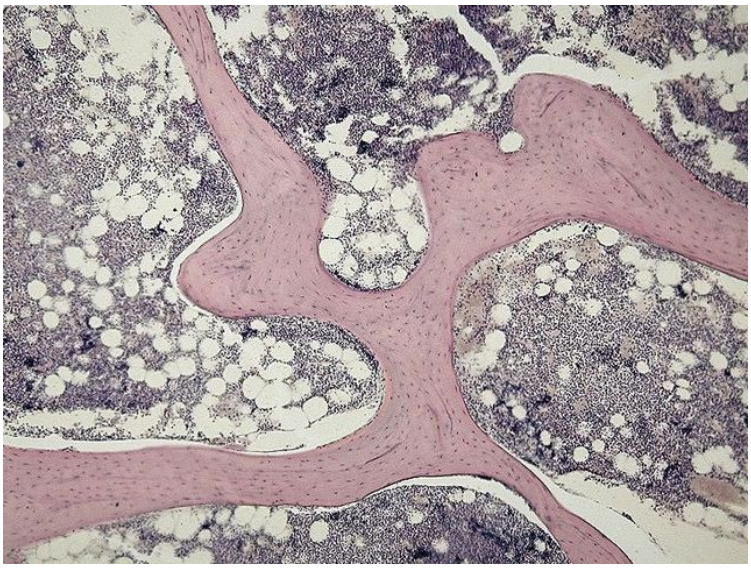

Figure 4: Light micrograph of cancellous bone[45]

2.2.3 Bone marrow

Bone marrow mainly lies within the trabecular bone, constituting nearly 4% of the total body mass on average. Red marrow, which consists mainly of hematopoietic tissue, and yellow marrow, made up of fat cells are the two types of marrow found in bone. Red blood cells, platelets, and most white blood cells are made in red marrow. In newborns, all such bones are filled exclusively with red marrow, but as the child ages it is mostly replaced by yellow, or fatty marrow. [46]

One of the main functions of bone marrow is a process called hematopoiesis, which creates red blood cells. The cells, which conduct this process, are called hematopoietic stem cells (HSCs). HSCs can replenish all blood cell types due to its multipotency. In order to maintain steady state levels in the peripheral circulation, approximately 10^{11}–10^{12} new blood cells are produced in red marrow daily,[47] using the bone marrow vasculature as a conduit to the body's system.[48] The number of HSCs in a healthy adult is never depleted due to its self-renewing ability.[49]This relies on both asymmetric and symmetric cell division.[50] These properties of multipotency and self-renewal are of key importance to the use for HSCs transplantation therapies. All the other tissues in red bone marrow not directly related to hematopoiesis are called stroma. However, stroma influences hematopoiesis indirectly by providing the microenvironment that facilitates hematopoiesis by the parenchymal cells. Stroma contains another important type of stem cell in bone marrow called mesenchymal stem cells (MSCs).[51]

HSCs have been used in bone marrow allogeneic transplantation for the treatment of patients with diseases of blood and bone marrow such as leukemia and multiple myeloma,[52,53] for more than30 years. HSCs studies through much of the past half century have led to a much

deeper understanding of their function. More recent advances have resulted in the use of HSC transplants in the treatment of cancers and other immune system disorders.[54]

In contrast, MSCs can differentiate into many types of cells including osteoblasts (bone cells), chondrocytes (cartilage cells), and adipocytes (fat cells). [55,56] Human clinical trials are still under way to use allogeneic MSCs for treatment a variety of conditions including myocardial infarcts, graft-versus-host disease, Cohn's Disease, cartilage and meniscus repair, stroke, and spinal cord injury and other diseases promised to use MSCs transplantation.[57]

The transplantation of bone marrow stem cells can be autologous and allogeneic. Autologous transplantation means that the stem cells were extracted from the patients themselves and stored in a freezer before use. High dose chemotherapy, sometimes with radiotherapy, is then used to treat patients with the intention of killing the malignant cell population, but unfortunately partial or complete bone marrow usually results. The stored stem cells are then transplanted into patients, replacing the destroyed tissue or restoring the normal blood cell production. However, in an allogeneic transplantation, the stem cells are donated to the recipient by a healthy person whose immune system markers closely matched to patients. The match is based on that the variability at three or more loci in the gene of HLA, a tissue type that is responsible for regulation of the immune system in humans.[58] A perfect match to the patients at these loci is preferred for a donor. However, immunosuppressive medication are still required for recipient to alleviate the graft-versus-host disease, a common complication following allogeneic transplantation, which usually does not happen in an autologous transplantation.[59] Donors are more likely matched to patients when they are related and a sibling is intentionally selected to match with patients and prevent inheritable disorders.

In general, compared to allogeneic transplantation, autologous transplantation has a lower risk of infection and very rare graft-versus-host disease incidence. These advantages lead to the widespread use of autologous transplantation in the treatment of lymphoma.[60] Research based on autologous transplantation is also being pursued as a cure for other diseases, such as myocardial diseases,[61] ischemic stroke,[62] myeloma,[63] and diabetes, [64]etc.

Even though autologous transplantation has many advantages, there are some diseases such as acute myeloid leukemia, for which the increased chance of cancer relapse for autologous transplantation makes allogeneic transplantation a better choice for patients even with a longer hospital treatment and the risk of peritransplantation death.[65,66] Taking this point into consideration, allogeneic transplantation appear to have higher possibility for curing long-term remission, once the short-term complications are prevented or mitigated.[67]

2.3 SCAFFOLD MATERIALS FOR HARD TISSUE

To reconstitute new tissue by cell based tissue engineering, three factors are necessary: 1) cells extracted from donors or the patients themselves, 2) scaffold substrates in which cells are cultured, and with which cells are implanted to fulfill desired function, 3) perfusion which controls the microenvironment promoting cells proliferation and differentiation of stem cells.[68] This section will discuss the scaffold used for tissue formation and growth, especially for bone and bone marrow.

The scaffold plays a role of providing a surface and void volume that improves the attachment, migration, proliferation and desired differentiation of stem cells and tissue progenitors. Based on the expected function of scaffold materials for tissue engineering,

biocompatibility and biodegradability is highly preferred.[69] While biocompatibility promotes cell-biomaterial interactions, biodegradability allows the replacement of the scaffold with natural biological tissues without leaving toxic degradation products. The degradation rate must match the new tissue generation time in order to maintain the structural integrity needed for tissue formation.[70] Porosity is also a requirement of the scaffold in order to provide sufficient accommodation for cell reproduction and differentiation that will eventually result in tissue formation. The interconnectivity between pores is also critical to uniform cell seeding and distribution, as well as for nutrients and metabolites exchange at the interface between the cells and scaffold.[71] The degree of scaffold porosity is found to be important in regulating the bioactivity of scaffold due to its influence on structural permeability, which controls the initial rate of bone regeneration, and the local mechanical environment, which mediates the equilibrium volume of new bone within the repair site.[72] Furthermore, as a mechanical support, the scaffold also needs adequate mechanical stability to undergo the implantation procedure and avoid collapse during the patient's normal activity. Other parameters influencing the efficacy of a scaffold include the pore morphology and the local environment in the area of the scaffold.[73]

Research activity related to the scaffold for bone tissue engineering has become very active. Some of these studies have made progress on manufacturing of scaffolds and some have been successful in specific application, even though most attempts have been plagued by poor implant survival and integration due to the lack of vascularization within the engineered bone constructs.[74]

The selection of materials for bone tissue engineering varies among metal, ceramics and polymer. The biocompatibility and utilization of all these materials has been researched and they all have demonstrated some advantages as well as some drawbacks. Metal such as titanium,

stainless steel and cobalt-chromium benefit from extraordinary properties of adequate biocompatibility, high strength and low cost.[75] Polymers are an alternative choice for scaffold due to their desirable properties, including biocompatibility, tunable degradation, processing ability, and versatility.[76]The composition of the inorganic mineral phase bone is approximated as hydroxyapatite (HA, chemical formula Ca_{10} $(PO_4)_6(OH)_2$ with a Ca/P ratio of 1.67)[77], and so ceramics have been widely considered as a material for bone tissue engineering scaffolds. Hydroxyapatite (HA) and tricalcium phosphate β-TCP are the two of most interest to researchers due to their similarity in structure and composition to the mineral phase of bone.[78] This gives HA and β-TCP high bioactivity and biocompatibility to bone and bone marrow cells, facilitating the attachment of progenitor cells seeded on the surface of scaffold and reproduction.[79] Nevertheless, HA and β-TCP are not suitable to some circumstance because of their low mechanical strength which may result in fracture.[80] HA also has a low degradation rate impeding the disappearance of scaffold and replacement by new tissue.

2.3.1 Hydroxyapatite

Hydroxyapatite (HA), with the formula of $Ca_5(PO_4)_3(OH)$, is a naturally occurring mineral form of calcium apatite. The formula is commonly written as $Ca_{10}(PO_4)_6(OH)_2$. For stoichiometric HA, the Ca/P ratio is 1.67 neglecting the substitution of any foreign ions in the lattice. For fully calcium deficient HA, the formula is $Ca_9(HPO_4)(PO_4)_5OH$. [81]

The crystal structure of HA is hexagonal with a space group of $P6_3/m$. Cell parameter is a=9.41 Å, c=6.88 Å with a/c=1/0.731 and a total of 44 atoms per unit cell. Calculated density of HA is $3.16 g/cm^3$, [82] Figure 5 shows unit cell of the structure of the HA crystal.

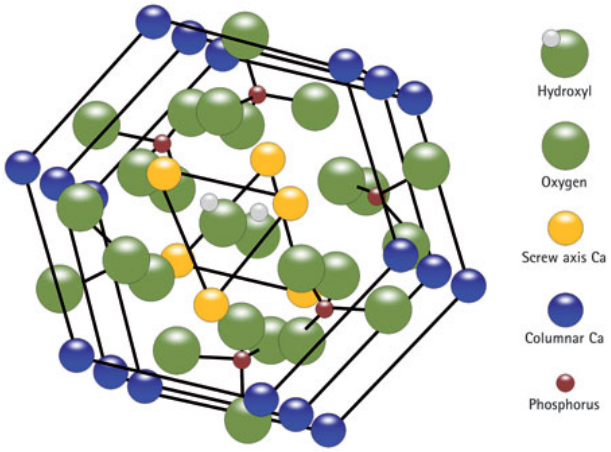

Figure 5: Crystal structure of Hydroxyapatite[83]

Hydroxyapatite is the hydroxyl endmember of the complex apatite group. It can form fluorapatite or chlorapatite when OH^{--} ion is replaced by fluoride, chloride or carbonate. The color of pure hydroxyapatite powder is white. Naturally existing HA can also show brown, yellow, or green colorations, comparable to the discolorations of dental fluorosis. HA is found contained in human teeth and bones. Up to 50% by volume and 7% by weight is a modified form of hydroxyapatite in bones.[84] Carbonated calcium-deficient hydroxyapatite is the main mineral of which dental enamel and dentin are composed.[85]

2.3.2 Tricalcium phosphate

Tricalcium phosphate(TCP) is one of phases of calcium phosphate, differing from Monocalcium phosphate and dicalcium phosphate in formula and crystal structure, Calcium phosphate refers to minerals containing calcium ions (Ca^{2+}) together with orthophosphates (PO_4^{3-}), metaphosphates or pyrophosphates ($P_2O_7^{4-}$) and occasionally hydrogen or hydroxide ions.[86] Common minerals of calcium phosphate have a formula of $Ca_5PO_4)_3\ \chi$. When χ is replaced by hydroxide (OH^-), it

becomes the formula of hydroxyapatite. The formula of tricalcium phosphate, $Ca_3(PO_4)_2$, consists of calcium ions (Ca^{2+}) and orthophosphates (PO_4^{3-}).

Different phases of TCP are stable at different temperature as shown on the phase diagram showed in figure 6. B-TCP has a rhombohedral structure with a space group of R3c that is stable up to 1125 ^{O}C. The monoclinic phase α-TCP, which has a complicated crystal structure with the space group of $P2_1/a$, is stable between 1125 ^{O}C and 1430 ^{O}C, and can be maintained to room temperature as a metastable phase. The α′-TCP is stable above 1430 degrees C and is unable to survive quenching to room temperature.[87]

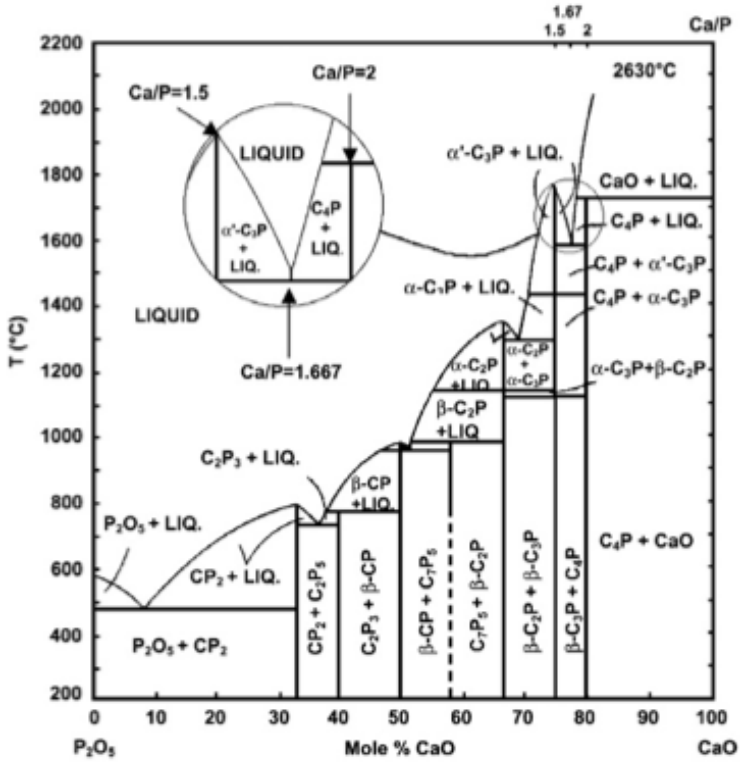

Figure 6: Phase diagram of the system CaO–P_2O_5 (C=CaO, P=P_2O_5) at elevated temperatures[88]

B-TCP can be described with a hexagonal unit cell whose parameters are a=b=10.4352Å, c=37.4029(5) Å, α=β=90°, and γ=120°.[89] It appears as white amorphous powder, with a

calculated density of 3,14g/cm^3, and solubility in water is 0.002 g/100 g.[90] The unit-cell parameters of α-TCP are, a= 12.8328 Å, b= 27.1958 Å, c= 15.1656 Å, α= γ =90°, and β= 126.2070°. The calculated density of α-TCP (2.8945 g/cm^3) is smaller than that of β-TCP, indicating the structure of α-TCP is more open. This loose structure is consistent with the higher reactivity of α -TCP in water and biodegradability.[91] Figure 7 shows the crystal structure of β-TCP, α-TCP, and α′-TCP.

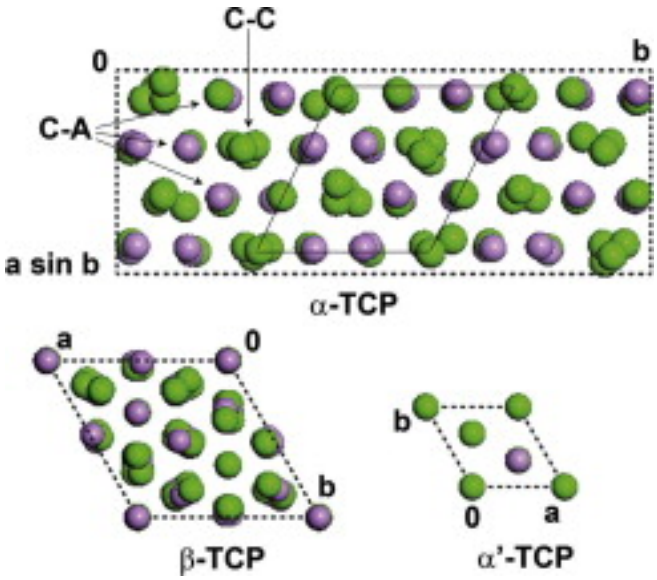

Figure 7: Schematic representation of the projections of the α-TCP, β-TCP and α′-TCP unit cells along the [0 0 1] direction[92]

In spite of having the same chemical composition, the medical application and manufacturing of biodegradable bioceramics shaped as dense and macroporous scaffold have primarily focused on β-TCP, while α-TCP is used more often as a fine powder in the preparation of calcium phosphate cements due to its higher solubility and reactivity.[93,94] Nevertheless, commercial bioceramic products made of α-TCP have been applied to bone repair and remodeling applications have used β-TCP and α-TCP materials.

2.3.3 Solubility of HA and TCP

The rate at which calcium phosphate scaffold materials will degrade is often measured, to a first approximation, in terms of their chemical solubility. The calcium ions and phosphate ions released during the process of dissolution from the scaffold into the solution has a critical influence on the culture environment. It is reported that calcium ions affect cells that reside in the bone marrow microenvironment or niche, such as osteoblasts.[95,96] So it is a necessary to have an understanding of the solubility kinetics of HA, and TCP.

The dissolution behavior of HA, β-TCP, α-TCP varies widely because of many factors, such as the method of preparation, phase content, density, the extent of ionic substitutions into the apatite lattice and microstructure.[97,98] However it is widely accepted that the order of solubility is α-TCP>β-TCP> HA.[99]

Figure 8 gives a comprehensive diagram of the solubility of different of calcium phosphates.[100] As a function of pH, the solubility of α-TCP, β-TCP, HA follow the order mentioned above over a large range of pH from 3 to 8. Monocalcium phosphate monohydrate, (MCPM) is not biocompatible and unsuitable to be used as a bone scaffold, due to its high acidity and solubility. The solubility of α-TCP, β-TCP, and HA is reviewed in a larger range of pH in the research of L.C. Chow.[101]

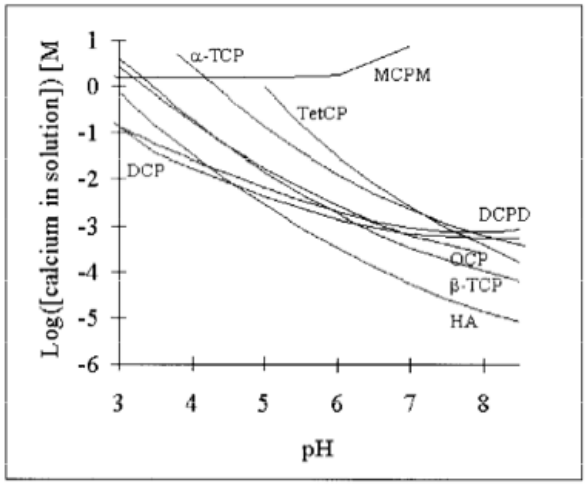

Figure 8: Solubility isotherms of several Calcium phosphates with different Ca/P ratio[102]

2.3.4 The application of ceramic scaffold

2.3.4.1 Bone cement The first bone cement appeared clinically for the first time in the 1940s in plastic surgery to close gaps in the skull. Early bone cement was nothing more than Plexiglas (i.e. polymethyl methacrylate or PMMA). The excellent tissue compatibility of PMMA allowed bone cements to be used for anchorage of head prostheses in the 1950s.[103] Bone cement combined with hydroxyapatite is also made for bone substitute and by regulating the size of HA particles, the ingrowth and attachment of bone tissue was promoted. However it is found that HA might have a negative effect on the mechanical properties of the scaffold.[104] Pure calcium phosphate bone cements first appeared in literature in 1980s. Unlike PMMA cements which harden through polymerization, calcium phosphate bone cements harden by mixing and dissolution of one or more calcium phosphate phases forming aqueous solutions and precipitating less soluble calcium phosphate phases. Generally the cement is a paste before setting, and so it has good moldability and injectability.[105] Gallinetti's research on biphasic

hydroxyapatite/β-TCP self-setting cements concluded that Ca^{2+} release and weight loss were unaffected by further increasing the amounts of β-TCP in the timeframe over which it was evaluated and there remains some doubt that higher dissolution and Ca^{2+} release might be observed in longer term study with high TCP content.[106]

2.3.4.2 Bioglass Bioglass is a commercially available family of amorphous bioceramics, usually having a composition with a different proportion of SiO_2, Na_2O, CaO and P_2O_5 and a high calcium/phosphorus ratio.[107]Bioglass scaffolds have been fabricated for bone tissue engineering by the method of foam-replication, using slurry-dip coating. Highly open, connected and porous scaffold have been made by this technique that show a great resemblance to trabecular bone.[108] .

Bioglass 45S5, Na_2O-containing bioactive glasses is one of the primary compositions used for research or clinical application in bone tissue scaffolds because it meets the basic requirement of mechanical strength and biodegradability, due to the formation of crystalline phase, $Na_2Ca_2Si_3O_9$.[109] One study by Qizhi Chen has explored the optimal fabrication process of 45S5 Bioglass scaffolds, based on a theoretical design combined with an experimental investigation,

New research shows that innovative bioactive glasses based on borate and borosilicate compositions have an ability to promote new bone formation and vascularization of new tissue when compared with silicate bioactive glasses.[108] The author speculates that this is facilitated by the rapid dissolution of the scaffold and consequent release of calcium into the microenvironment of the tissue. If the dissolution it too fast the build up of non-physiological elements such as boron and sodium can be toxic to the cells.[110] Borate-based bioactive glasses are able to control the rate at which the degradation of implant occurs to make it compatible with

the rate of new bone formation.[111] Other studies of bioactive glasses are reviewed in the work of Rahaman.[94]

2.3.4.3 Biphasic calcium phosphate bioceramics In general, HA have difficulties in degradation after implantation.[112] On the other hand, β-TCP scaffolds have lower strength and biocompatibility compared to HA with same porosity. So the use of crystalline calcium phosphate-based bioceramics remains challenging. Biphasic calcium phosphate, consisting of certain proportions of HA and β-TCP, is one common approach to addressing this problem. Biphasic calcium phosphate have been optimized to eliminate the drawbacks of pure HA or β-TCP as a bone tissue scaffold. The different ratio of HA/β-TCP can alter the rate of degradation according to the work of Daculsi G.[113] Biphasic calcium phosphate is also found to have the ability to form a layer of carbonate-apatite on their surface, which provides chemical bonding between the implants and newly forming bone.[114] They also can be made to be osteoconductive with the appropriate macroporosity and microporosity.[115]

Noticing that bone, in fact, resembles as a mix of inorganic HA matrix and organic collagen fibers,[116] methods of using calcium phosphate-based bioceramics combined with polymers have been studied. The incorporation of polymer in CaP scaffolds can increase toughness and compressive strength and result in mechanical behavior similar to bone. Successful scaffolds, combining HA with chitosan-gelatin,[117] PLA,[118] PLGA,[119] and collagen,[120] or TCP coated by PCL,[121] PGA[122] have been shown to enhance bone formation in vitro and/or in vivo.

2.4 PROCESSING OF MACROPOROUS CERAMICS FOR SCAFFOLDS

As discussed above, the porosity and pore size are two key parameters concerning the efficacy of ceramic scaffold for tissue engineering. The necessity for porosity will be summarized and several methods for making macroporous ceramics will be reviewed.

Traditionally, pores are avoided in ceramic materials because of the flaw sensitivity of brittle failure, not commonly shared by metallic and polymeric porous structures.[123] However, many areas of application, including the bone tissue engineering, require highly porous ceramics. Kuboki showed the necessity of pores in bone tissue scaffolds by proving that no new bone formed on solid particles of HA in a rat ectopic model, while direct osteogenesis occurred in porous scaffolds of HA. This is because pores with suitable size and connectivity facilitate the migration and proliferation of the two kinds of bone stem cells and new-formed osteoblasts.[124] Furthermore, the porous structure has been proven to be contributive to the mechanical interlocking between implant scaffold and natural bone, providing greater mechanical stability at this critical interface.[125]

Generally, porous materials are classified into three categories depending on the pore diameter d: macro-porous (d>50 nm), meso-porous (50 nm>d>2 nm) and micro- porous (d>2 nm), according to the IUPAC (International Union of Pure and Applied Chemistry).[126] For bone tissue scaffold, the minimum pore size required to generate mineralized bone is considered to be 100μm according to the research of Hulbert et al.[127] He also concluded that larger pore size resulted in more substantial bone ingrowth, while scaffold with smaller pore size resulted in the growth of unmineralized tissue or fibrous tissue.

The influence of other parameters related to porosity is shown in the work of Hing, who suggested that there is no optimal porosity standard that guarantees the rapid osteointegration in

ceramic scaffolds, however, there are broad guidelines for making bone tissue ceramic scaffold, which includes a minimum of 50%-60% in porosity and a pore size larger than 100μm.[128]Karageorgiou has published a review on the influence of porosity on osteogenesis, concluding that high porosity and large pores enhance bone ingrowth and osteo-integration of an implant after surgery. The minimum recommended pore size for a scaffold is 100μm, which correspond to Hing's statement. Additionally, he suggested that high degradation rate materials should have porosity lower than 90%, since the mechanical and structural integrity tend to be compromised by rapid degradation.[129]

The porosity and pore size are significantly influenced by the processing method used for manufacturing the porous ceramics. Partial sintering is the most straightforward processing route for the preparation of porous ceramics..[130,131] However, this method result in relative low porosity (<60%) which is not high enough for bone tissue ingrowth. Therefore, innovative processing methods that can tailor porosity are required for making ceramic scaffold for bone tissue engineering. Figure 9 shows the porosity and the average pore size can be obtained by a variety of forming methods. Three general methods can be used to make macroporous ceramics, and they are reviewed below. [132,133,134]

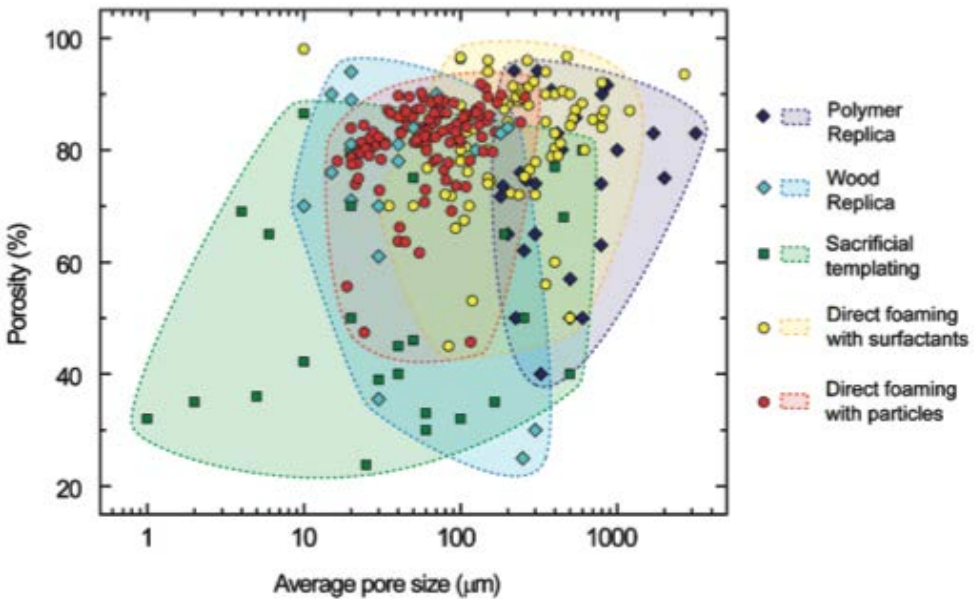

Figure 9: Typical porosity and average pore size achieved via the replica, sacrificial templating, and direct foaming processing routes[135]

2.4.1 Foam Replication

This approach begins with the coating of a template porous cellular structure with a ceramic suspension, a precursor solution, etc. The template used could be a porous polymeric sponge such as polyurethane,[136] or a piece of wood which is initially soaked in a ceramic suspension until the internal pores are coated in with ceramic material. After that, roller compression is applied to the coated sponge to remove the excess suspension, and subsequently dried and pyrolyzed through careful heating. Finally, sintering at temperature ranges from 1100°C to 1700°C is usually required to densify the final foams. In this process, the appropriate viscosity and fluidity of the ceramic suspension are required so that uniform ceramic layer forms over the sponge walls. Figure 10 (a), schematically shows the process of foam replication. Natural sources, such as woods,[137] corals[138] can function as the solid template.

Porous ceramics obtained with foam replication can reach total open porosity levels within the range 40%–95% and are characterized by a reticulated structure of highly interconnected pores with sizes between 200μm and 3mm.[139]In addition, a variety of ceramic cell types could be formatted, including open- cells, semi-closed cells and closed cells.[140]However, during the pyrolysis of the polymeric template, the reticulated ceramic structure are often cracked, significantly degrading the mechanical strength of the final porous ceramics. This is the major disadvantage of the foam replication process.[141]

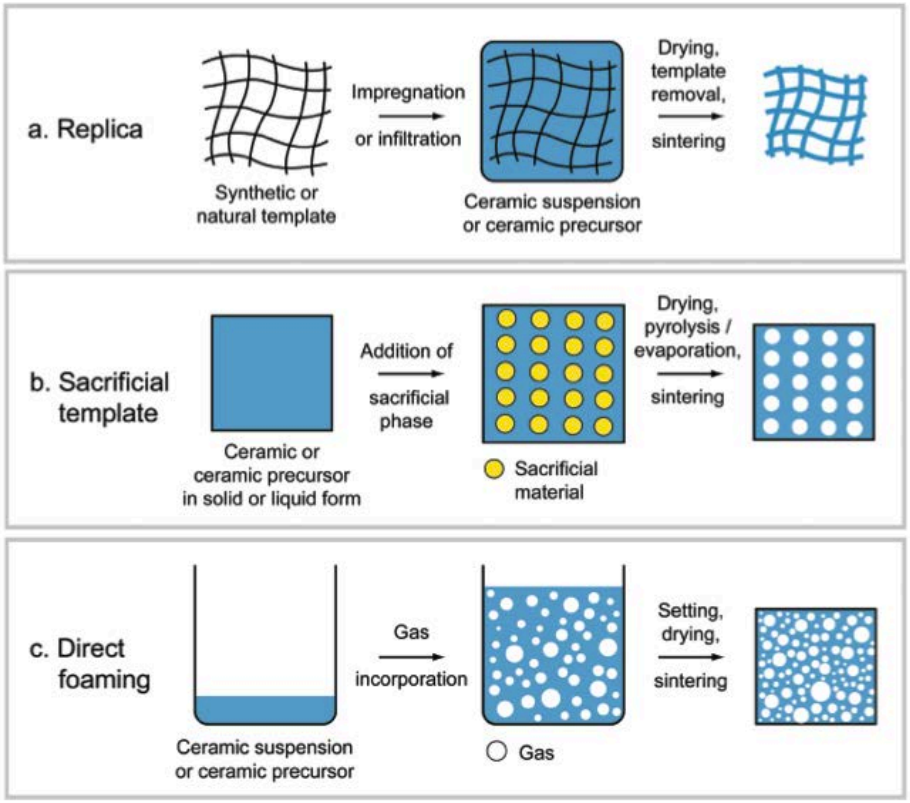

Figure 10: Possible processing routes used for the production of macroporous ceramics[142]

2.4.2 Sacrificial template foaming

This method starts with a preparation of a biphasic composite consisting of a continuous ceramic phase of particles or precursors as a matrix and a homogeneously dispersed sacrificial phase which is eventually extracted to form pores within the structure. Figure 10 (b) schematically shows the process of this method. The sacrificial phase is usually polymer beads, organic fibres, potato starch, graphite, charcoal, salicylic acid, etc.[143,144,145] These foaming agents are usually classified into organic matter, inorganic matter and liquid. Organic agents are often extracted through pyrolysis by applying long thermal treatment at temperature between 200°C-600°C.[146,147] The extensive amount of gaseous by-products and mismatch in thermal expansion coefficient caused by the long period of pyrolysis of the organic component are the main disadvantages of organic agents and they can induce cracks within the porous structure. Inorganic agents, on the other hand, are usually eliminated by chemical means. For instance, salt crystals are removed simply by washing the composite with water repeatedly.[148]Fibers agents need more aggressive liquid like acid leaching. [149]

Porosity is controlled by the amount of the agents, and pore shape and size are also affected by the shape and size of the agents respectively when their sizes are large in comparison with those of starting powders or matrix grains. This approach is useful particularly for obtaining high open porosity. The range of porosity and pore sizes that can be achieved with this technique is very broad (20%–90% and 1–700 mm, respectively), as they only depend on the volume fraction and size of the sacrificial template used.

2.4.3 Direct foaming

In this method, the porous structure is formed by incorporating air or easily-evaporated liquid into a prepared ceramics suspension which are stabilized to prevent pores from growing too big and coalescing. Subsequent drying and sintering is also required to obtain the final structure. The general process is shown in figure 10 (c). Other than air, liquid used to form the porosity include: alkane,[150] CO_2,[151] ethanol,[152] etc. The porosity of direct foamed ceramics is proportional to the amount of gas incorporated into the suspension during the foaming processing.

Liquid foams such as those produced by these direct foaming methods are thermodynamically unstable due to their high gas-liquid interfacial area, causing three physical processes: drainage, coalescence, and Ostwald ripening. Drainage is the physical separation between the gaseous and liquid phases of the foam because of the effect of gravity, resulting a denser foam layer on the top and heavier liquid phase in the bottom. The bubbles at top are characterized as highly packed foams with very thin film between touching cells. Coalescence happens after foam drainage since the thin film are no longer stable enough to keep touching cells apart, resulting the association of neighboring bubbles. The mechanism of Ostwald ripening is generated by the difference in Laplace pressure between bubbles of different size, where the Laplace pressure means the pressure difference between the inside and the outside of a curved surface.[153] This difference in Laplace pressure of distinct sized pores leads to the steady diffusion of gas from smaller to larger bubbles with time, thereby causing Ostwald ripening. These destabilization processes quickly increase the size of pores in the foam structure. However, an introduced surfactant that increases the stability of the bubble surfaces can be very useful for impeding these process because of the attachment of surfactant to the air water interface, decreasing the interfacial energy of gas-liquid boundaries.

Therefore, direct foaming with surfactants requires a setting agent or drying to consolidate the foam microstructure before extensive coalescence can take place. The ultimate pore size of the porous ceramic depends on a balance between the kinetics of bubble coarsening and the speed of liquid/suspension setting or drying. A variety of surfactant have been researched and been developed to make porous ceramics by direct foaming. Lipids and proteins are two common groups of surfactants, others include sodium dodecyl sulfate and benzethonium chloride. This surfactant based foaming method can achieve a pore size ranging from 35μm to 1.2mm and a porosity of 40% up to 97%. Either closed or opened pores with a spherical shape can be obtained, based on adjusting the foam stability, air content, particle concentration and setting kinetics. Furthermore, this method usually results in dense flawless struts after sintering, increasing markedly the mechanical strength of the porous ceramic in comparison with foam replication method.

Studies have shown that solid particles with tailored surface chemistry can also be used to stabilize bubbles.[154,155] Particles absorbed at the interface of gas/liquid are proven to efficiently impede the destabilization processes described above for days, unlike only minutes or hours of stabilization time provide by long-chain surfactant and protein surfactant.[156] Particle stabilized foams typically have a porosity from 40% to 93%, whereas the average pore size can be obtained is only about 10 to 300 μm. Closed pores structure and thin cell wall usually expected in the product of this method. However, by decreasing the concentration of stabilizing particles, open pores structure can also be prepared.

2.5 SINTERING

Sintering, a process of forming a solid material from powders by heating at a certain temperature lower than the melting point, is usually required in the preparation of bioceramic scaffold. Through sintering, a strengthening and densification of the ceramic take place, caused by a reduction in porosity and reduction in volume (sintering shrinkage). Chemical reaction may be also involved in sintering, changing the chemical or phase composition in the final product. Therefore, a detailed understanding of ceramic sintering is of importance, because the final mechanical properties and biological behavior of the ceramics significantly depend on this process. A specific review about the sintering of hydroxyapatite and tricalcium phosphate is presented below.

The sintering of HA is generally performed in the temperature range from 1100°C-1250°C.[157] The fact that no secondary phase, either crystalline, amorphous or liquid are formed during the process of sintering HA in this range of temperatures has been proved.[158] Even though Raynaud claimed that HA decomposes into TCP and HA above 900°C, and inverse phase change (TCP to HA) occurs during cooling process,[159] most studies on this subject agreed that HA remain stable up to 1350°C -1450°C.[160,161] Only a partial transformation of hydroxyapatite to oxyhydroxyapatite proceeds above 900°C.[162]

Commonly 3 stages are involved in the sintering of HA. At low temperature from 400°C up to 700°C-800°C, the surface area of HA powders begin to decrease without densification, leading to little consolidation of the initial powder compact. The second stage starts at approximately 750°C, when thermal energy provided is enough to active the volume or boundary diffusion required for densification. Densification occurs by the shrinking of the pores, which corresponds to an increase in relative density to 90%. The final stage happens when all the pores

are isolated and begin disappear and leave a fully dense ceramic. There is usually some residual porosity.[163,164]

The sintering of β-TCP is more complex compared to HA, for it is reported that β-TCP is only thermodynamically stable at low temperature and transforms to α-TCP at the temperature range from 1120°C -1170°C.[165] According to the research of Ryu,[166] the relative density of sintered β-TCP increased rapidly to 83% below 1150°C and then α-TCP was observed above 1200°C. The relative density continued to increase, but slowly due to phase transition, and reached to 95% at 1550°C, (figure 11) even though, α-TCP was present only as a minor phase. This behavior creates two difficulties in sintering β-TCP. Firstly, the low mechanical reliability due to the porosity due to the reduction in densification rate associated with the phase transformation. Another issue is that the reverse transformation from α-TCP to β-TCP during cooling process does not go to completion resulting in unwanted α-TCP in the cooled ceramics.[138] To overcome this difficulty, additives are used to increase high-temperature limit of β-TCP. These additives, including MgO,[167] ZnO,[168] and $Ca_2P_2O_7$,[147] etc., are chosen because of their tendency to improve biological or mechanical properties.

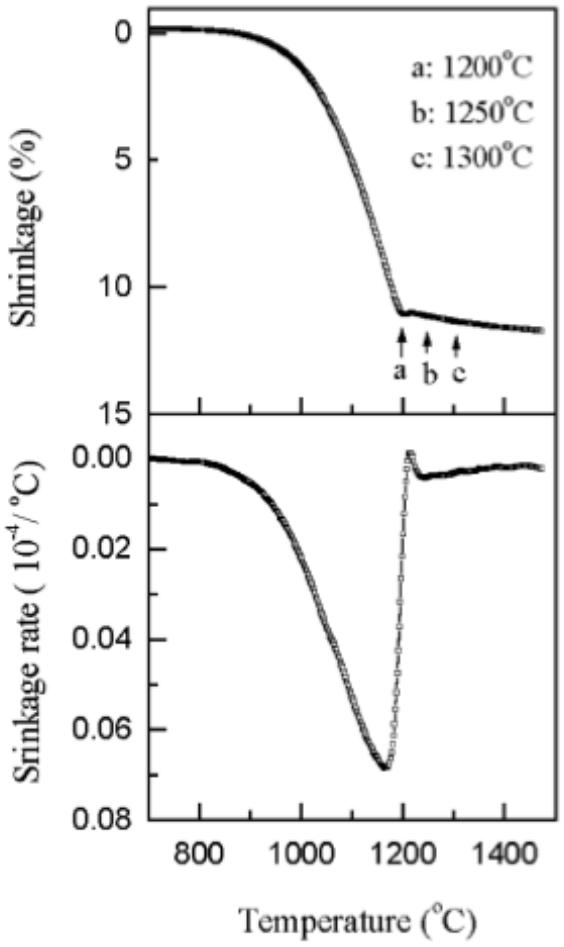

Figure 11: Shrinkage and shrinkage rate of the pure b-TCP sample at each temperature[169]

The sintering process of biphasic calcium phosphates (BCP) ceramics is also well studied. Higher temperatures are required at least 800°C for the onset of densification and at least 1250°C is required for fully dense.[170] Mg is usually added to prevent phase transformation from β-TCP to α-TCP, allowing BCP be sintered at high temperature without forming α-TCP.[171] Raynaud, summarized the sintering characteristics of BCP with various Ca/P ratio, concluding that BCP with a high amount of β-TCP has significantly lower linear shrinkage when sintered, while BCP with low amount of β-TCP (<30wt%) did not result in much transformation from β-

TCP to α-TCP and has a linear shrinkage smaller than pure HA but larger than BCP with a high amount of β-TCP.[172]

2.6 INFILTRAION

Infiltration is a process of introducing a second phase into a porous ceramic by being immersed in a precursor liquid that is decomposed into an inorganic phase upon heating. The pre-infiltrated ceramic must have open-pores structure with a relatively high porosity, allowing liquid flows through most of the pores. Therefore, a partial sinter process at a lower temperature is needed to shape a pre-infiltrated ceramic materials with a relatively low density compared to those fully dense ones.[173]Through the infiltration process, unique microstructure, surface modification, compositional gradient, and mechanical properties can be achieved, as long as suitable second phases are selected and their spatial distribution is carefully controlled. [174] Some of the infiltration studies are summarized below.

Honeyman-Colvin infiltrated alumina powder compacts with mullite, stabilized zirconia and partially stabilized zirconia, finding that all of these second phases contribute to a higher strength of the materials.[153] Interestingly, in the work of Yung-Jen Lin', mullite was infiltrated into zirconia, demonstrating that the porosity and pore diameter is decreased after infiltration with minor improvement in hardness and no improvement in fracture toughness.[175] This may be due to the fact that the final infiltrated ceramic was still porous. Glass, infiltrated porous zirconia with molten nitrate salts found that the infiltration depth is a function of both the infiltration time and the initial relative density of the pre-infiltrated ceramics. The study also developed a modified form of Darcy's law to predict infiltration depth.[154] Another study used mullite

precursors to infiltrate alumina, and concluded that a concentration gradients (the mullite content decreasing with increasing distance from the surface of the ceramics) resulted. Additionally, a microstructural effect (the alumina grain size in composite bodies tended to increase with distance from the surface of the sample) was observed. These studies support the idea that infiltration is an effective means of tailoring the composition and microstructure of ceramic bodies.[176]

Research had been conducted concerning the influence of Ca content on the degradability of HA.[177] Since Infiltration is a method capable of manipulating the Ca content in ceramic scaffold, Ca infiltrated ceramics provides a promising method to optimize calcium phosphate ceramics.

3.0 HYPOTHESIS

β-TCP has become one the most popular choice for bone tissue scaffold due to its fast dissolution rate compared to hydroxyapatite.

Recent study has suggested that a higher calcium concentration in hydroxyapatite scaffolds based on hydroxyapatite might improve the degradability of the scaffold.[178] However, the influence of Ca concentration on the degradability of scaffold made by β-TCP has not been researched yet.

Also, according to the review of Alexander Hoppe, higher Ca concentration enhances ostegenesis and angiogenesis,[179] while some other researches prove that high Ca content also hinders the function and differentiation of bone marrow stem cells.[180,181]

Therefore, the hypothesis of this work is that a degradable TCP scaffold with enhanced calcium release, due to a CaO introduced by infiltration of porous TCP, can be produced without exceeding the commonly recognized Ca ion limit of 3mol/L.

Objectives.

1. Process a composite of β-TCP and CaO by direct foaming, infiltration and insitu formation of CaO.
2. Study the effects of reaction between β-TCP and CaO, and the possible formation of hydroxyapatite.

4.0 APPROACH

4.1 MATERIAL PREPARATION

4.1.1 β-Tricalcium phosphate powder

The β-TCP powder used is a laboratory product (product number 21218) from Sigma-Aldrich. The purity of it reaches as high as 96%. The trace elements are listed in table 1.

Table 1: List of trace elements in β-TCP powder

anion traces	chloride (Cl^-): ≤500 mg/kg
	sulfate (SO_4^{2-}): ≤1000 mg/kg
cation traces	Cd: ≤50 mg/kg
	Co: ≤50 mg/kg
	Cu: ≤50 mg/kg
	Fe: ≤200 mg/kg
	K: ≤100 mg/kg
	Na: ≤1000 mg/kg
	Ni: ≤50 mg/kg
	Pb: ≤50 mg/kg
	Zn: ≤50 mg/kg

4.1.2 High calcium content pellets

The β-TCP powder was pressed into 13mm diameter pellets at a pressure of 30MPa. The average green density of the pellets was 58.7%.

According to the $CaO–P_2O_5$ phase diagram, β-TCP transforms to α-TCP at nearly 1200℃, which makes it difficult for β-TCP to be fully densified. To investigate the influence of sinter temperature on the transformation from β-TCP to α-TCP and densification, the pressed pellets were first sintered at temperature from 1000°C to 1300°C (one temperature point every 50°C) for an hour using a heating rate of 5℃/min and a cooling rate of 10℃/min. The bulk relative density of the each pellet sintered at different temperature was determined using the Archimedes method with 4-5 repeats for each condition. The true density of β-TCP used was 3.07g/cm^3. This procedure was used to establish the pre-sintering temperature prior to infiltration and the final sintering temperature after infiltration.

Once the sintering temperature range had been established, pressed pellets were sintered at 3 different temperatures: 1200℃, 1250℃, 1300℃ for different times. Relative bulk density of samples under each condition was determined with 4-5 repeats. Table 2 lists all the conditions were used to treat pressed pellets.

Table 2: Heat treatment parameters used for the sintering of pressed pellets

	0.5h	1h	2h	5h
1200℃				
1250℃				
1300℃				

The high calcium content pellets were prepared by infiltrating Ca into partial sintered pellets. Calcium nitrate tetrahydrate ($Ca(NO_3)_2 4H_2O$,Alfa Aesar, England) was used as a source of calcium. Dissolved by water, solutions contain $Ca(NO_3)_2 4H_2O$ with Ca^{2+} concentration of 0mol/L, 1mol/L, 2mol/L were prepared. Partial sintered pellets were put into these solutions and evacuated to remove air from the pores in the pellets. After 24 hours, the pellets were taken out from the calcium nitrate solution and immersed in ammonium hydroxide solution with pH=12-13 for 30 minutes to form $Ca(OH)_2$ insitu in the pores and on the external surfaces of the pellet. Then the pellets were pre-fired at 900℃ in order to crystallize the CaO in the infiltrated pellets. By now, the pellets had higher ratio of Ca/P than pure β-TCP(Ca/P=1.5).

Similarly with un-infiltrated pellets, infiltrated pellets were then sintered at temperature of 1200℃, 1250℃, and 1300℃ for 2 hours to investigate the influence of sintering temperature on infiltrated pellets. The heat rate was 5^{O}C/min while cooling rate was 10^{O}C/min. The control group (infiltrated with 0mol/L) samples were made in the same processing steps except for infiltration.

4.1.3 High calcium content β-TCP foam

The foam of β-TCP were made by emulsion method and infiltrated to obtain high calcium content ceramic foam by an emulsion based direct foaming method. Ammonium polymethacrylate polyelectrolyte dispersant (Darvan C,RT Vanderbilt Co.) was added to deionized water, with pH=5.5 adjusted by HCl solution. Then the β-TCP powder was added to the water gradually while the suspension was being slowly blended. After all the powder was added, the blending speed was raised to 2500RPM and continued for 20 minutes to realize a fully dispersed suspension. After that, a cationic surfactant (benzothonium chloride, sigma) was used

added and mixed at 2500RPM for 2 minutes to stabilized the following foaming process. Finally, 10% volume of heptane was added and mixed at high speed for 2 minutes. The recipe for making the foams is listed in table 3.

Table 3: The recipe for making porous β-TCP foam

Volume% of β-TCP	36%
Mass of β-TCP	12g
Darvan C	3.48ml
Deionized water	3.47ml
Alkane	1.2ml
Benzothonium Chloride	0.0883g

Since humidity is a major parameter determining the foam expansion, the final emulsion was poured into a paper cup mold and placed in an incubator with a humidity of 65% for approximately an hour and the suspension was allowed to foam. The humidity was decreased after 1 hour to nearly 35% until the foam fully dried without collapsing, which usually took 24 hours. The dried emulsion, with the paper cup mold, was then fired in furnace at $900^{O}C$ with a heating rate of $5^{O}C$/min and a cooling rate of $10^{O}C$/min.

To make infiltrated foams, the foams firstly partial sintered at $1100^{O}C$ for an hour to obtain a suitable strength for infiltration. The infiltration process is also similar to the process applied to the pellets: after infiltrated with Ca^{2+} concentration of 0,1, and 2 mol/L, the foams were immersed in ammonia hydroxide with pH=12-13 and then pre-firing at $900^{O}C$. Finally, the foams are sintered at a relatively high density at $1200^{O}C$ for 2 hours with a heating rate of $5^{O}C$/min and a cooling rate of $10^{O}C$/min.

4.2 CHRACTERIZATION METHOD

4.2.1 Relative bulk density measurements

The relative bulk density was measured based on the Archimedes' principle that the upward buoyant force is equal to the weight of the fluid that the immersed body displaces. The procedures were described as below.

After taking out from the furnace, the mass of the sintered pellets (4-5 repeats) was immediately measured as M_a. The pellets were placed in beaker and immersed in water, Along with the beaker, they were put into a container, which was then evacuated to remove air from the pellets using an air pump for 30 minutes. The pellets were immersed for 24 hours in order that all air in the pellets was removed. The beaker was taken out from the container, and the mass of pellets when immersing in water was measured as M_b.

Then the pellets were taken out from the beaker. The surface of the pellets was gently wiped using lab tissue, to remove excess water attached on the surface while preventing the water actually inside the pellets from being removed. The mass of each pellet was measured afterwards as M_c

According to Archimedes' principle,

$F_{buoyancy}=\rho_{water}gV=\rho_{water}gM_a/\rho_{TCP}=M_cg-M_bg$

$\rho_{TCP}=\rho_{water}M_a/(M_c-M_b)$The true density of β-TCP used is 3.07g/cm^3

The relative bulk density was then calculated by $\rho=\rho_{TCP}/\rho_{true}$.

4.2.2 XRD analysis

For the samples without infiltration, both the surface and cross-section of the pellets sintered at different temperature were scanned by x-ray to identify potential second phase such as α-TCP. The scanning angle ranges from $20°<2\theta<80°$ according to the standard pattern of α-TCP and β-TCP as shown in figure 12 (a), (b). The peaks used to identify α-TCP are the main peak ($2\theta=35.80°$) and several low density peaks ($26°<2\theta<29°$), as marked in figure 12 (b). Noticing that no peaks of α-TCP appear above $2\theta=50°$, more detailed scan were achieved, by narrowing down the range to $20°<2\theta<50°$ and increasing scanning time to obtain more accurate peak pattern.

For the infiltrated pellets, as well as scanning the sintered surface and cross-section of the samples, the pellets were ground into powder and scanned to obtain more average analysis. Several possible second phases, including CaO, $Ca(OH)_2$, $CaCO_3$, and HA might exist or co-exist in infiltrated pellets after sintering. The overall name of all these second phases (not including α-TCP) is termed as "Ca-rich phases. Due to the fact that α-TCP might be formed in the infiltrated pellets after sintering, the characterized peaks for the Ca-rich phases should not overlap with the peaks of either the β-TCP or α-TCP. By comparing those standard pattern as shown in figure 12 (a), (b), (c), (d), (e), (f) the peaks identifying each phases were found except for CaO:

$Ca(OH)_2$: $2\theta=33.34°$, and $2\theta=20.82°$; $CaCO_3$: $2\theta=33.89°$; HA: $2\theta=37.16$.

The diffraction pattern of CaO shows that only few characterized peaks existing for CaO and they are overlapped with the peaks of β-TCP or α-TCP, which makes it hard to identify CaO phase.

Based on the study of the standard diffraction pattern, the scanning angle range for infiltrated pellets were set to be from $2\theta=15°$ to $2\theta=45°$.

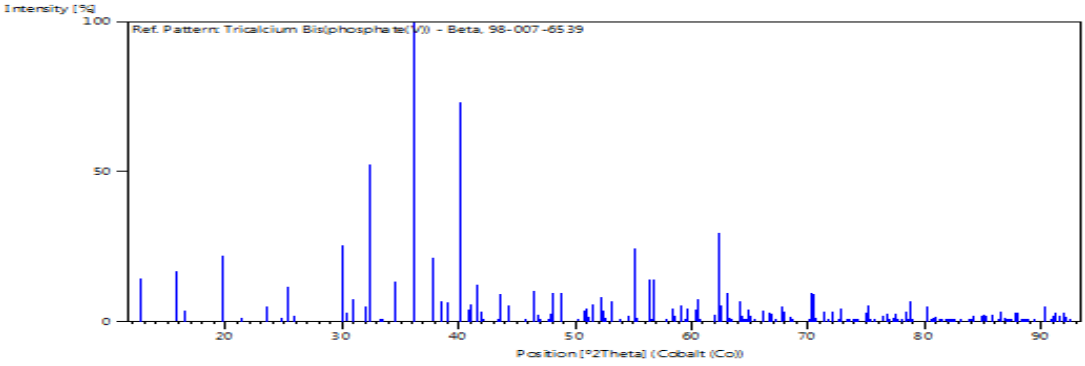
Intensity [%]
Ref. Pattern: Tricalcium Bis(phosphate(V)) - Beta, 98-007-6539
Position [°2Theta] (Cobalt (Co))

(a)

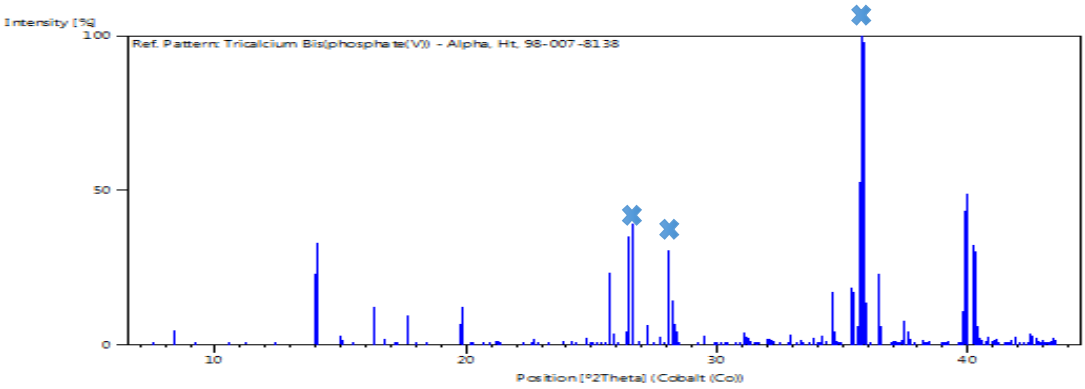
Intensity [%]
Ref. Pattern: Tricalcium Bis(phosphate(V)) - Alpha, Ht, 98-007-8138
Position [°2Theta] (Cobalt (Co))

(b)

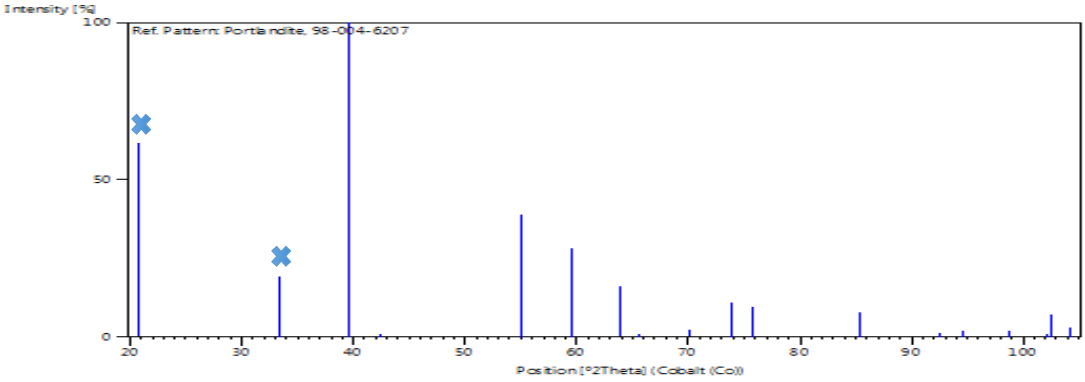
Intensity [%]
Ref. Pattern: Portlandite, 98-004-6207
Position [°2Theta] (Cobalt (Co))

(c)

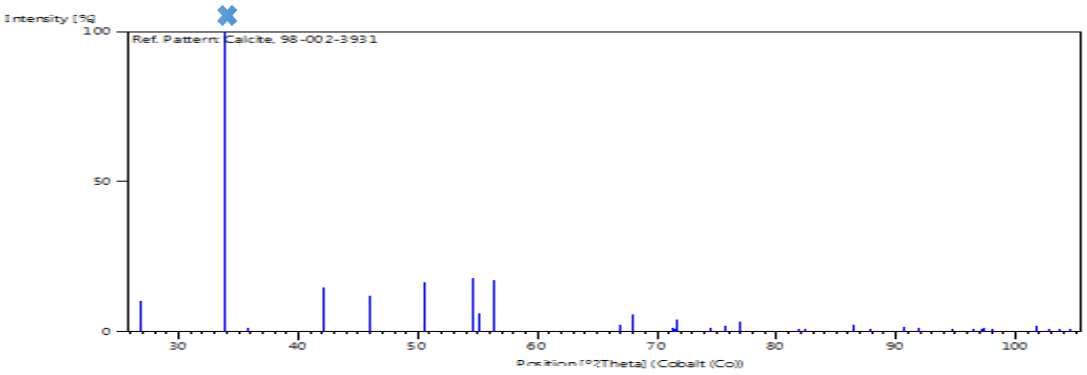

(d)

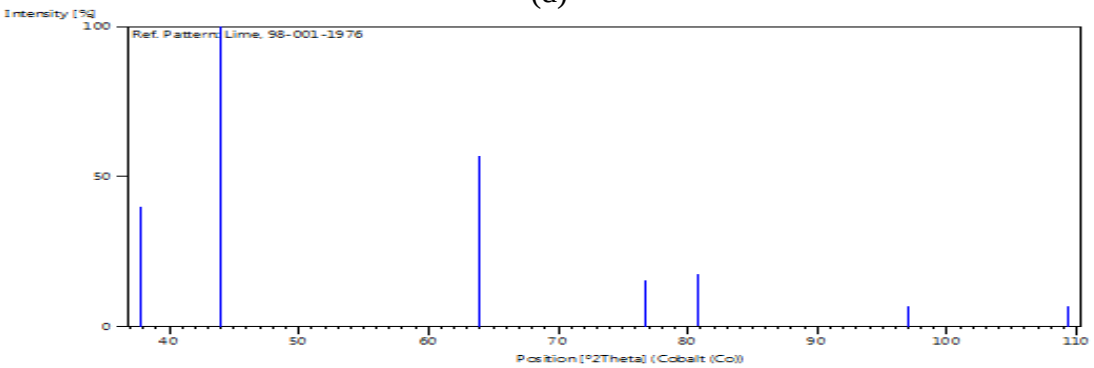

(e)

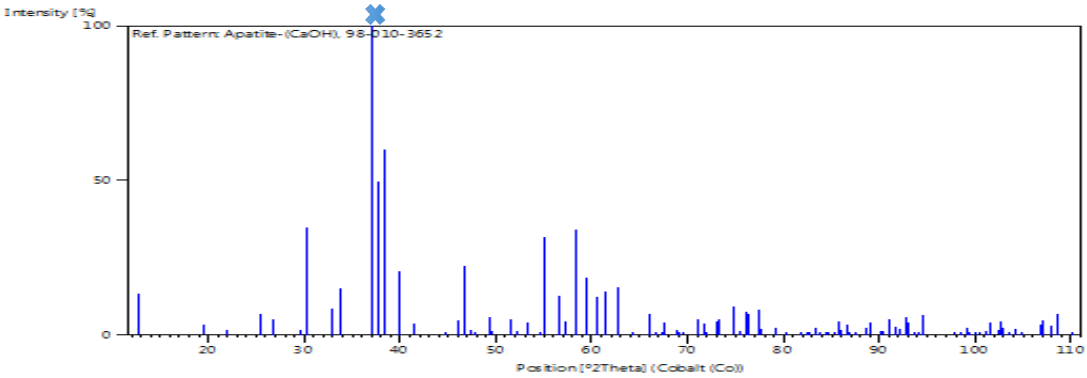

(f)

Figure 12: The standard X-ray diffraction pattern of (a) β-TCP, (b) α-TCP, (c) $Ca(OH)_2$, (d)$CaCO_3$, (e)CaO, (f)Hydroxyapatite

4.2.3 SEM observation

Scanning electron microscopy analysis was done on the surface and cross-section of β-TCP pellets treated under different infiltration and sintering conditions, in order to investigate the influence of sintering parameter and calcium infiltration on them. These samples prepared by impregnating into low viscosity resin and oil-polished by the process shown in table 4.

Table 4: Procedures of preparing SEM samples

Steps	Diamonds sized/μm	Loading/lb	Speed/rpm	Media
1	45	18	60	Water
2	30	18	60	Water
3	15	17	70	Polish oil and paste
4	6	16	50	Polish oil and paste
5	1	16	50	Polish oil and paste

After polishing, the samples are sonicated in alcohol to remove the impurities, such as oil or paste, without causing any defects on the surface. Furthermore, a control group of infiltrated pellets were prepared by ultra-sonicating in water for 5 minutes to create defects introduced by the Ca-rich phases, since CaO, $CaCO_3$ and $Ca(OH)_2$ are much more soluble in water than TCP. Finally, all samples were coated with palladium using Cressington sputter coater/108auto and observed in Joel 6610-LV under 15kV or 20 kV.

The foams subjected to solubility testing (which will be discussed in the following section) were also observed in SEM to investigate the microstructure and dissolution behavior with different immersion times and different concentration of infiltrated calcium.

4.3 SOLUBILITY PROPERTY EXPERIMENT

Three groups of infiltrated foams with 0mol/L, 1mol/L, 2mol/L Ca^{2+} infiltration were prepared as the procedures described in 4.1.3. Afterwards, they were placed separately in sealed tubes which contained 25ml Tris-buffer Saline (TBS). Seven time points were set to each group, listed in table 5, and one foam from each group is removed at every time point. After the removed foams were fully dried, they were coated with palladium and observed in SEM.

Table 5: Time points for each group under infiltration process with different Ca concentration

	0.5hr	1 hr	1day	3days	1 week	2 weeks	4 weeks
0mol/L							
1mol/L							
2mol/L							

5.0 RESULTS AND DISCUSSION

5.1 SINTERING BEHAVIOR OF B-TCP PELLETS

Previous studies have shown that the powder preparation method, the ratio of Ca/P, and the addition of substituted ion can significantly affect the sintering behavior of β-TCP.[182,183,184] Sintering behavior curves

Figure 13 shows the relative density of pressed β-TCP pellets sintered at 1000°C 1050 °C, 1100 °C, 1150 °C, 1200 °C, 1250 °C, 1300°C for 1 hour, using a heating rate of 5°C/min and a cooling rate of 10°C/min. As can be seen from the figure 13, the level of the densification increases gradually from 1000°C to 1300°C. However, the slope of the curve suggests that the inflection occurs at approximately 1250°C when sintered for 1 hour. The highest relative density obtained after 1 hour of sintering was 88.5% and the TCP never reached final stage sintering (92%). This result is thought to be due to the disruptive volume change on the β-TCP to α-TCP transformation at sintering temperatures of 1250 °C and above, since the density of α-TCP(2.87g/cm^3 is lower than the density of β-TCP(3.07g/cm^3. The shape of the curve in figure 13 is similar to the sintering curve reported in Hyun-Seung Ryu's paper.[158] Main difference is that the inflection occurs at 1150 °C in this previous report, while at 1250 °C in the curve showed here. The difference in the sinterability of the powders may be responsible for the different observations but the inability to reach high sintered density was a common observation

in this study and the study of Hyun-Seung Ryu et al. Furthermore, for the purposes of the consequent infiltration in this work, the relative density of pellets sintered at 1100°C for 1h was approximately 64%, which was considered a suitable density for infiltration because of the large fraction of porosity and the fact that all the pores remain connected to the surface. So the partial sintering conditions for the powders set to be at 1100°C for 1h.

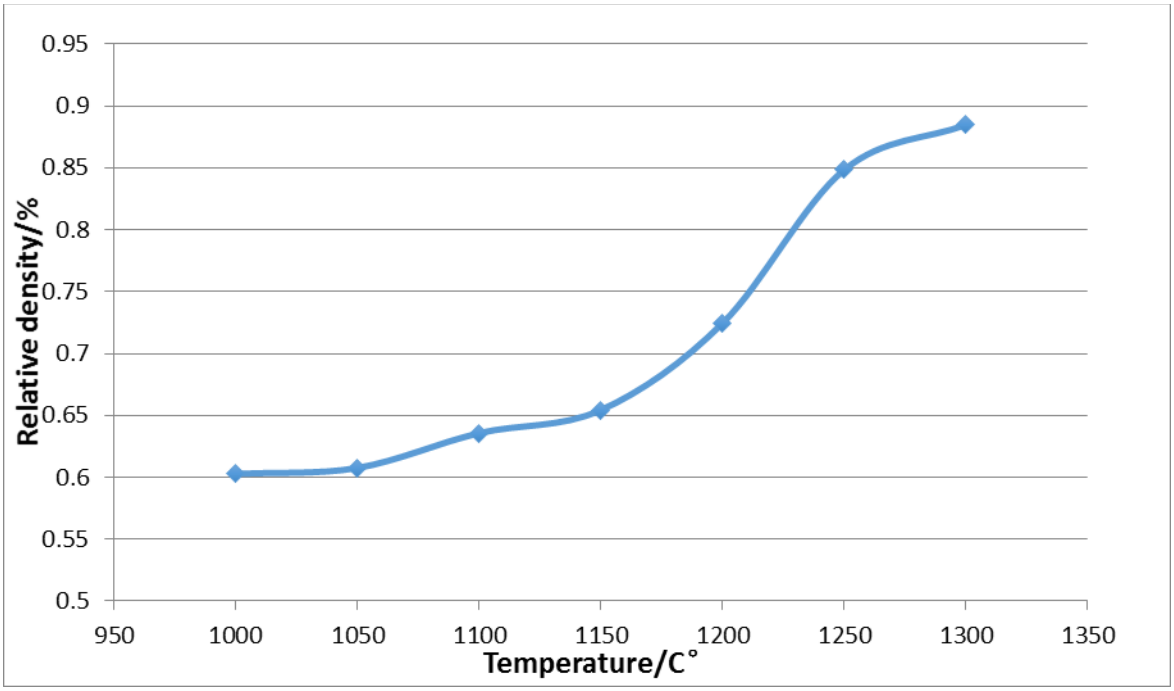

Figure 13: The plot of relative density vs temperature for β-TCP pellets without infiltration

The relative density of sintered pellets under 12 different heat treatment conditions were measured, and its mean values and standard deviations were listed in table 6. Figure 14 integrates the results in the table 4 into 3 curves to show the trends and differences more directly. It is well known that, for most ceramics, the relative density increases with log (sintering time) until fully densified. With this in mind the results are discussed below.

The trend of the relative density of pellets sintered at 1200°C shows the expected trend with time. The highest relative density was only 80% at this temperature. The trend suggests that

little or no α-TCP phase formed was formed such that the sintering was unaffected. The curve of the pellets sintered at 1250°C undergoes a slight decrease from 87.5% at 0.5h to 85% at 1h and then increase to 86% at 2 hours and 89% at 5 hours. The initial decrease is unexpected, but might be caused by the formation of α-TCP. Since that the standard deviation of relative density for the sample sintered at 1250°C, 1hr) is about 3%, the decrease is assumed to be caused by variations between the samples repeats and the curve may have a slowly increasing trajectory limited to approximately 90% by slow sintering kinetics in this density range, little α-phase formation is thought to have occurred at this temperature. In contrast, sintering behavior of pellets sintered at 1300°C exhibits opposite trend with a relatively high density of 89% after 0.5 hours and a gradual decrease to 85% at 5 hours. Considering the standard deviations, the relative density remains unchanged at this temperature or decreases slightly at longer sintering times. Again high density was not achieved, perhaps due to the transformation of β-TCP to α-TCP that was shown to occur in the pellets sintered at 1300°C. The highest relative density reached is 89.3%, which is still not high enough to be considered as final stage densification.

Table 6: The mean values and standard deviations of the tested relative densities

	0.5h		1h		2h		5h	
	Mean	SD	Mean	SD	Mean	SD	Mean	SD
1200°C	69.5%	0.0064	72.4%	0.0029	74.6%	0.0039	80.4%	0.0085
1250°C	87.5%	0.0073	84.8%	0.0357	86.4%	0.0063	89.3%	0.0141
1300°C	89.0%	0.0133	88.5%	0.0141	86.1%	0.0040	84.8%	0.0355

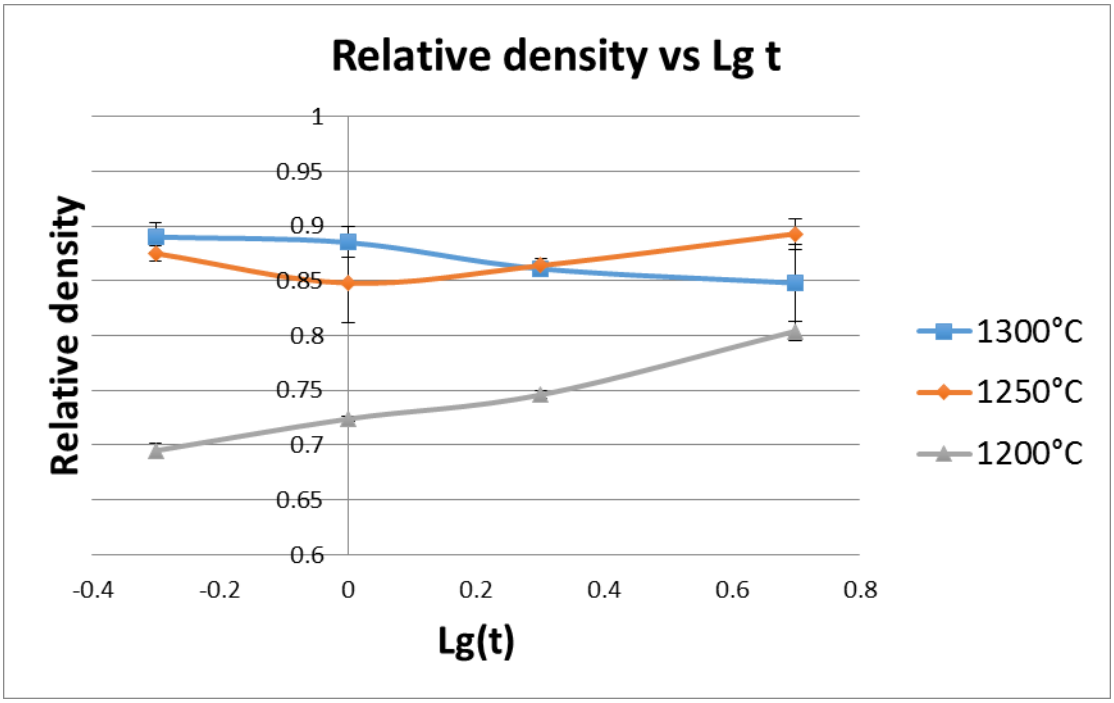

Figure 14: The curves of relative density vs lg (t) at 3 different temperature

5.1.1 SEM observation

Figure 15 (a), (b), (c) displays the morphology of the surface of the pellets sintered at 1300°C for 1h, 2h, and 5h. It is can be seen that the morphology of the surface of the pellets undergoes significant changes along with time. The pores between the TCP grains coarsened during sintering with increasing sintering time. This would explain why the sintered density does not increase above 89%, the pore coarsening process produces fewer more widely spaced pores thereby increasing the diffusion distance and slowing the sintering process. The reason for the pore coarsening is unclear. It may be caused by coarsening of the grain structure during sintering or may be associated with the phase transformation from β-TCP to α-TCP if the α-phase shows faster coarsening. Similar changes of morphology are also found between pellets sintered at different temperature for the same time. As can been seen in figure 15 (d), (e), (f), the

higher the sintering temperature, the larger the pores that created by the process of sintering. In summary, the results above demonstrates that the relative density of pellets sintered at 1200°C is lower than those at 1250°C and 1300°C as expected but it undergoes the expected increase in density on sintering. At the higher temperatures the pore structure coarsens considerably and limits the density to less than 90%. It is now necessary to determine the phase distribution to see if the pore coarsening correlates with the formation of α-TCP.

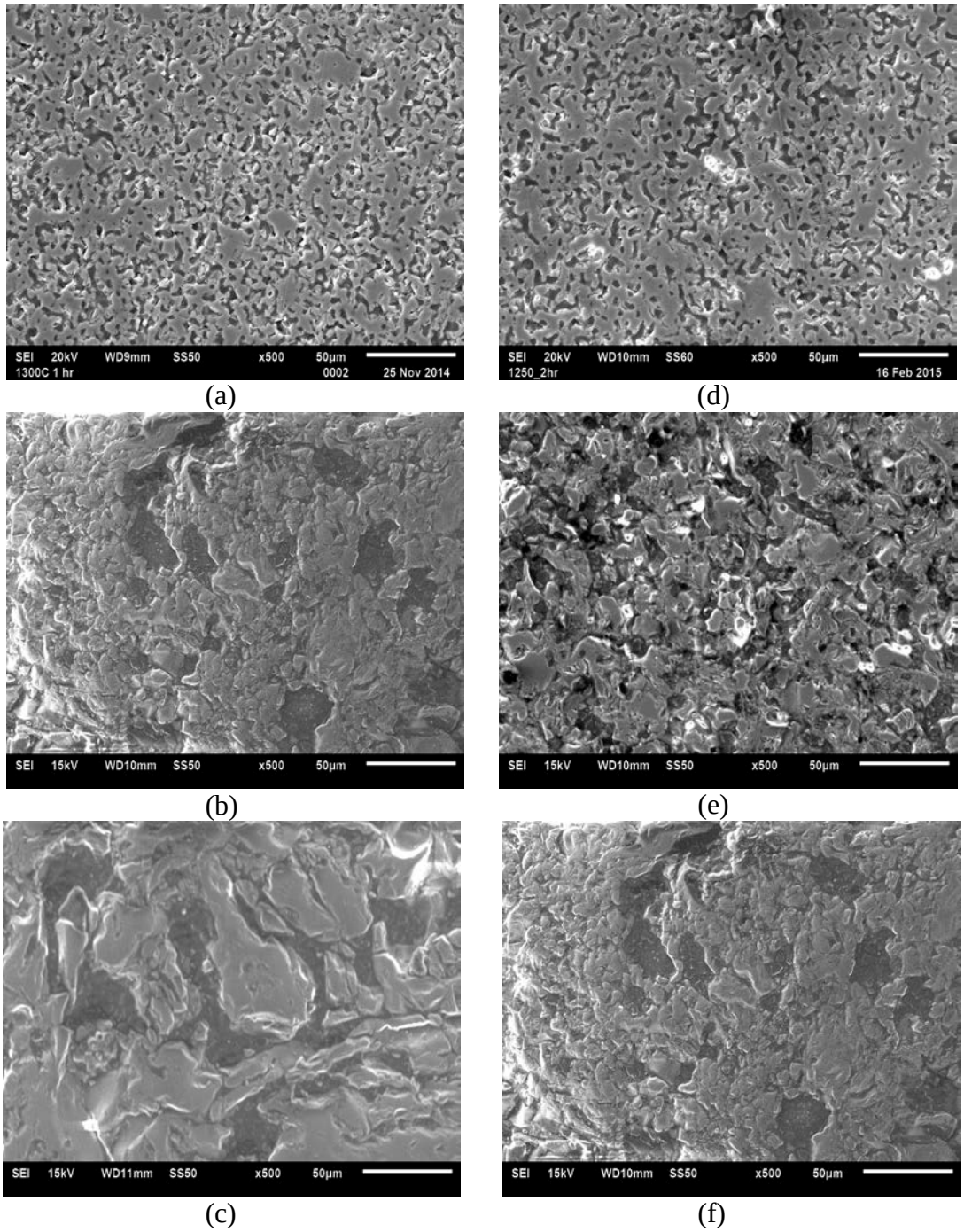

Figure 15: SEM image of the surface of pellets sintered at 1300°C for (a)1h, (b)2h, (c)5h and pellets sintered for 2 hours at (d)1200°C, (e)1250°C, and (f)1300°C

5.1.2 XRD analysis

To identify the α-TCP phase in the samples, the x-ray diffraction patterns of the sintered pellets at different temperature (1200°C, 1250°C, 1300°C) for 2 hours were studied. Due to strong relationship between the crystals structures and the numerous reflections observed for β-TCP and α-TCP, most of their peak overlap. Previous studies often used the main peak of α-TCP (2θ=35.8°) and several other peaks with relatively low intensity (range from 25°<2θ<29°) to qualitatively determine the relative amounts of α-TCP and β-TCP. The diffraction patterns of each pellet sintered at different temperature are nearly the same, and it is found difficult to identify α-TCP, even in the diffraction pattern of the pellet sintered at 1300°C. Amplified pictures of the pattern derived from these pellets, as is shown in figure 16, demonstrates that the peaks to identify α-TCP (green lines) were not present in the pattern. The main peak of α-TCP(2θ=35.8°) does not appear to contribute to the nearby peak of β-TCP and the peaks ranging from 26° to 29° do not appear either.

These results are contradict to the expected transformation to α-TCP when sintered above a temperature of 1125°C according to P_2O_5-CaO diagram and the previous report by Hyun-Seung Ryu et al. The potential reason for this might be a very low content of α-TCP was formed in this study, so that the x-ray signal is not strong enough to differentiate the nearby overlapping peaks, noticing that the main peak of α-TCP(2θ=35.8°) is close to the second highest peak of β-TCP(2θ=36.1). Also, considering the fact that the surface of the pellets is not as flat as a polished surface and might cause high noise to signal ratio at lower angle, including the minor α-phase peaks from 25°<2θ<29°.

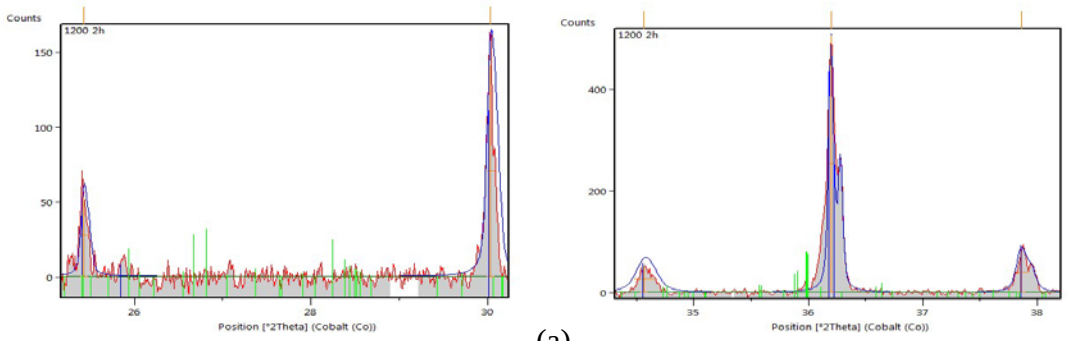

(a)

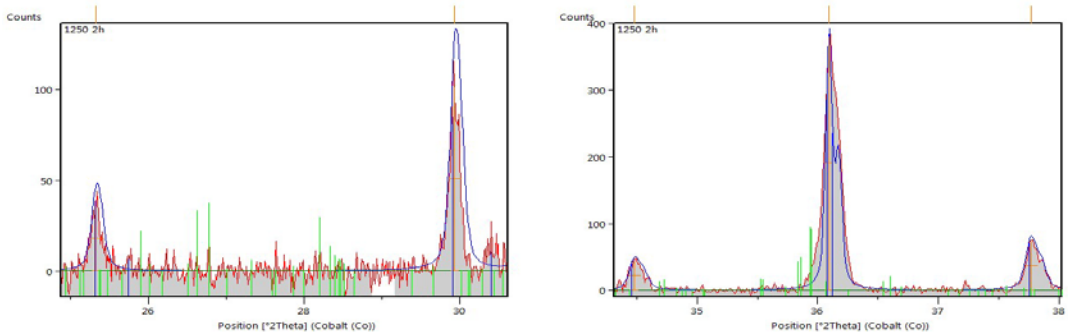

(b)

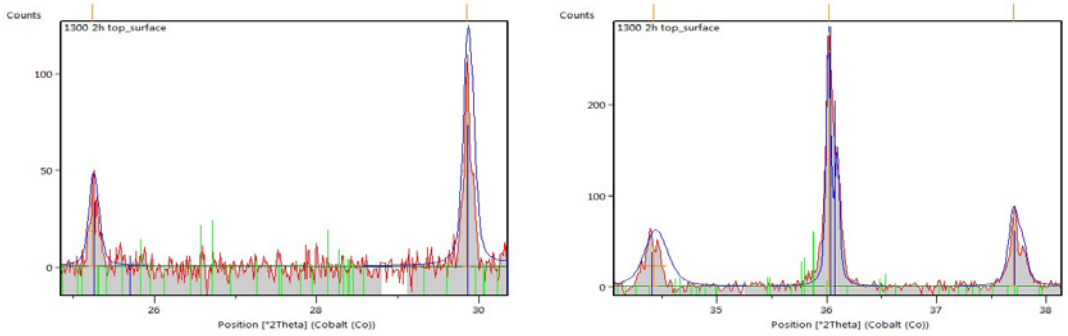

(c)

Figure 16: Diffraction patterns of the surface of pellets without Ca infiltration sintered for 2 hours at (a)1200°C, (b)1250°C and (c)1300°C

Therefore, the signal count was improved by increasing the scanning time and narrowing the step size, in order to obtain more accurate diffraction pattern of pellets sintered at each temperature. However, the evidence for the existence of α-TCP has not yet to be found in the un-infiltrated pellets sintered at any of temperature (1200°C, 1250°C, and 1300°C). The diffraction pattern of the pellet sintered at 1300°C with a more detailed scan is shown in figure 18. Still, the

α-TCP is not well identified, for the peaks of α-TCP (green lines) are not showed up in the pattern. The diffraction patterns of pellets sintered at 1200°C and 1250°C by more detailed scan were obtained but are not shown here since they are similar to the results shown in figure 17.

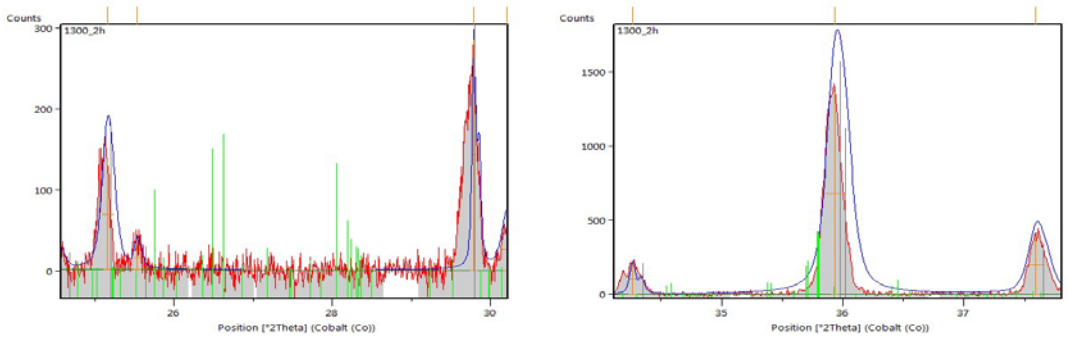

Figure 17: Detailed scan of surface of pellet without Ca infiltration sintered at 1300°C for 2h

However, compared to diffraction pattern of pellets sintered at 1300°C showed in figure 16 (c), the peak at 2θ=36° derived from the higher resolution scan pattern does shift to the position of the main peak of α-TCP (2θ=35.8°), which can be regarded as a possible evidence for the existence of α-TCP, suggesting that, at least, very small amount of α-TCP might exist. The shift may also be caused by the exact positioning of the sample surface in the beam and so there is no evidence of α-TCP in the un-infiltrated pellets. According to the paper of R.G. Carrodeguas et al,[185] it is also possible that any α–TCP formed during sintering transformed back to β-TCP on cooling from the sintering temperature due to a low cooling rate.

Additionally, the cross-section of the pellets sintered at each temperature were x-rayed as well, since there might be a difference in proportion of each phases at surface or at interior. However the diffraction pattern obtained shows no differences from the pattern obtained from the sintered surface, as can be seen in figure 18.The diffraction patterns of pellets sintered at 1200°C and 1250°C but they show similar results.

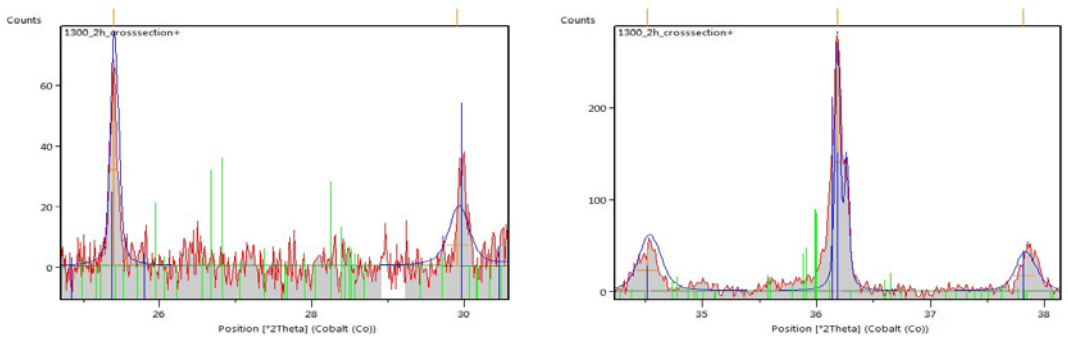

Figure 18: Diffraction patterns of cross-section of the pellet without Ca infiltration sintered at 1300°C for 2 hours

In summary, the transformation from β-TCP to α-TCP may be the cause of the pore coarsening observed at the high sintering temperatures and many researches have same conclusion.[158, 159,186] However, this study cannot confirm the formation of α-TCP at higher sintering temperatures that is predicted by phase diagram and the conversion to α-TCP is very small under the experimental conditions used and it is difficult to be detected by XRD. Interestingly, another report, by M. Bohner et al[187] stated that little conversion from β-TCP to α-TCP were found in β-TCP samples with a slightly lower ration of Ca/P (1.47<1.50) when it is sintered at 1300°C for 2 hours. These findings are very similar to the data collected here. The material used here could be calcium deficient.

According to the P_2O_5-CaO phase diagram shown in figure 19, in Ca-deficient TCP will form a liquid phase when sintered at temperature above 1288°C, while the melting point for calcium phosphate with a ratio of Ca/P=1.5 is 1470°C and in Ca-rich region, liquid phase will not appear until the sintering temperature reach 1578°C. To clarification, TCP is a line compound, Ca-deficient TCP means TCP containing a second phase with lower Ca/P ratio (<1.5) and Ca-rich means TCP containing a second phase with higher Ca/P ratio (>1.5). There is no pure TCP that is Ca-deficient or Ca-rich. From the observation of macroscopic observations of

the pellets produced in this study, as shown in figure 20 the pellets sintered at 1300°C are appear to have distorted under gravity which may indicate melting. Pellets sintered at lower temperature do not have such change in shape. Returning to the SEM images shown in figure 15, the observed pore coarsening at the longer sintering times might be associated with the formation of a small amount of liquid phase that is not detectable by XRD analysis. To examine this further TCP pellets were infiltrated with calcium to increase the Ca/P ratio and thereby avoid the possible formation of a liquid phase if the TCP is calcium deficient. These experiments will be described in the next section.

The powder used for this dissertation is a β-TCP product with a purity of 96%, and other amorphous calcium phosphate with lower ratio of Ca/P might result from powder synthesis and result in calcium deficient powder.

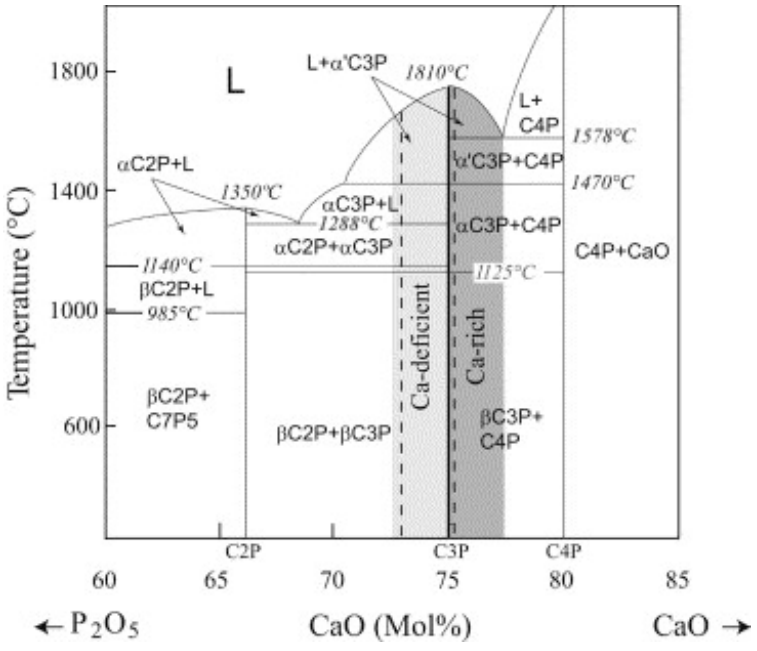

Figure 19: A detailed part of P2O5-CaO phase diagram

Figure 20: Pellets sintered at 1300°C (Right) and 1250°C (Left) from different direction

5.2 INFILTRATION PROCESSING

After treated in ammonium hydroxide solution and sintering, the introduced calcium might exist in air at room temperature as in the form of CaO or $Ca(OH)_2$. $CaCO_3$ also has a possibility of existing in the final products, due to the reaction between CO_2 in the air and $Ca(OH)_2$. Therefore several calcium rich phases could be present. Additionally, TCP would be expected to react with CaO at the sintering temperatures used to form hydroxyapatite (HA). All these phases will be termed as Ca rich phases in the following discussion.

5.2.1 SEM observation

Since the possible second phases, including CaO or $Ca(OH)_2$ and $CaCO_3$, have a much higher solubility in water than β-TCP and α-TCP, water-treating the SEM samples would be an effective method leach these phases from polished surface and quantify the resultant damage. The SEM images of the surface of the 2mol/L infiltrated pellets sintered at 1200°C, 1250°C and 1200°C are collected in figure 21, both with and without exposure to water during polishing.

Comparing the SEM images of the pellets sintered at 1200°C, there is little difference and no apparent defects were created by water treatment. Careful observation of the images of

samples sintered at 1200^{O}C suggested that there may be some small defects in the water treated pellets. This might indicates that, at least, particles at the surface are removed by the water treatment. For the pellets sintered at 1250°C and 1300°C, the water-treated samples show significant difference in contrast to the oil-polished (no water treatment) samples. Defects were created after water treatment as is shown in figure 21(d) and (f). However, the size of these defects are large, and therefore it is likely that the defects might not only a result from individual grains of Ca rich phases (CaO, $Ca(OH)_2$, or $CaCO_3$), but also of removal of adjacent TCP crystal that are coordinated to Ca(CaO, $Ca(OH)_2$, or $CaCO_3$) particles.

To make it more certain the defects were caused by infiltrated Ca (CaO, Ca $(OH)_2$, or $CaCO_3$) phases, the cross-section of the infiltrated pellets were observed under SEM. It is expected that the infiltrated Ca (CaO, $Ca(OH)_2$, or $CaCO_3$) phase has a gradient with higher concentration on or near the infiltrated surface and lower concentrations in the interior. Figure 22 shows the images of the cross-section of the infiltrated pellets sintered at 1300°C. Figure 22(a), (b), and (c) are taken from top surface, interior, and bottom surface, respectively. The defects (white contrast) exists throughout the cross-section of the sample but are more concentrated near the infiltrated surface. In other words, a gradient does exist as expected. However, the size of the white defects changes and looks different from the ones in the images taken from the surface of the infiltrated pellets directly. This may be due to the constrained growth of the crystals for the calcium rich phases in the interior of the pellets.

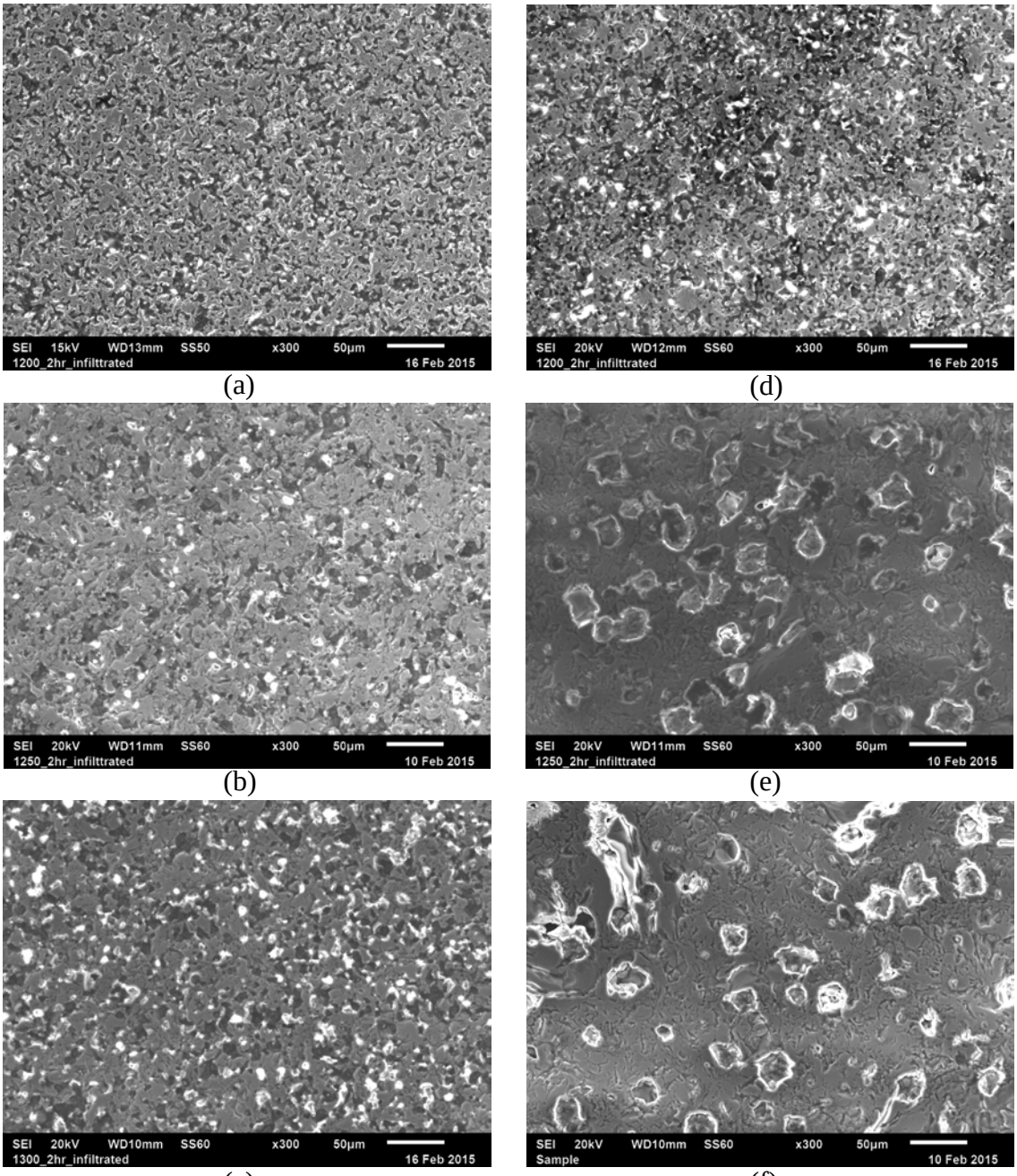

Figure 21: SEM Images of infiltrated pellets sintered at (a)1200°C without water treated (oil polished), (b)1200°C with water treated, (c)1250°C without water treated, (d)1250°C with water treated, (e)1300°C without water treated, and (f)1300°C with water treated

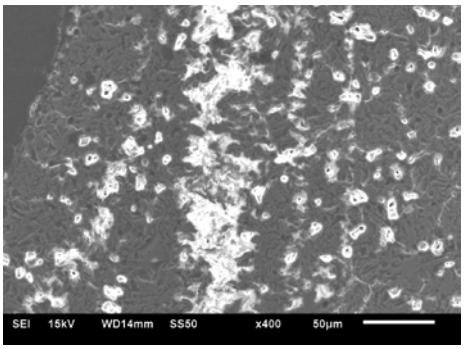

(a)

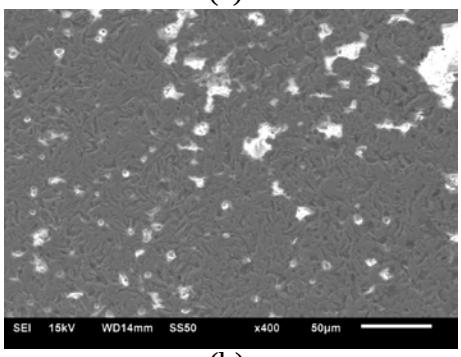

(b)

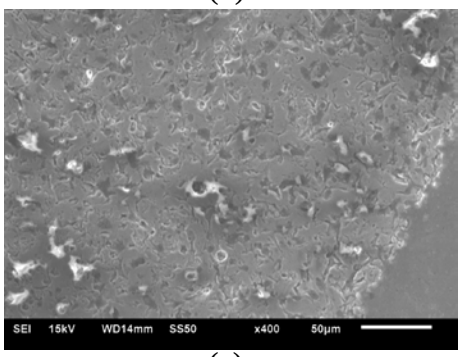

(c)

Figure 22: SEM images of the cross-section of the infiltrated pellets sintered at 1300°C for 2hrs

Finally, the images of oil-polished infiltrated pellets (Figure 21(a), (c), (e)) and the images of un-infiltrated pellets (Figure 15(d), (e), (f)) were compared (as shown in figure 23). They were attached below for convenience. For pellets sintered at 1200°C, the morphology of the microstructures looks the same with or without Ca infiltration. However, for the pellets sintered at 1250°C and 1300°C, the morphology of the infiltrated one seems less coarse and looks similar to the pellets sintered at lower temperature (1200°C), while significant coarsening happened in the un-infiltrated ones when sintered at 1250°C or 1300°C. As discussed in 5.1, this phenomenon could be explained by that melting happened in the un-infiltrated pellets, while this does not happen in the infiltrated pellets, since the main difference between infiltrated pellets and un-infiltrated pellets is the ratio of Ca/P.

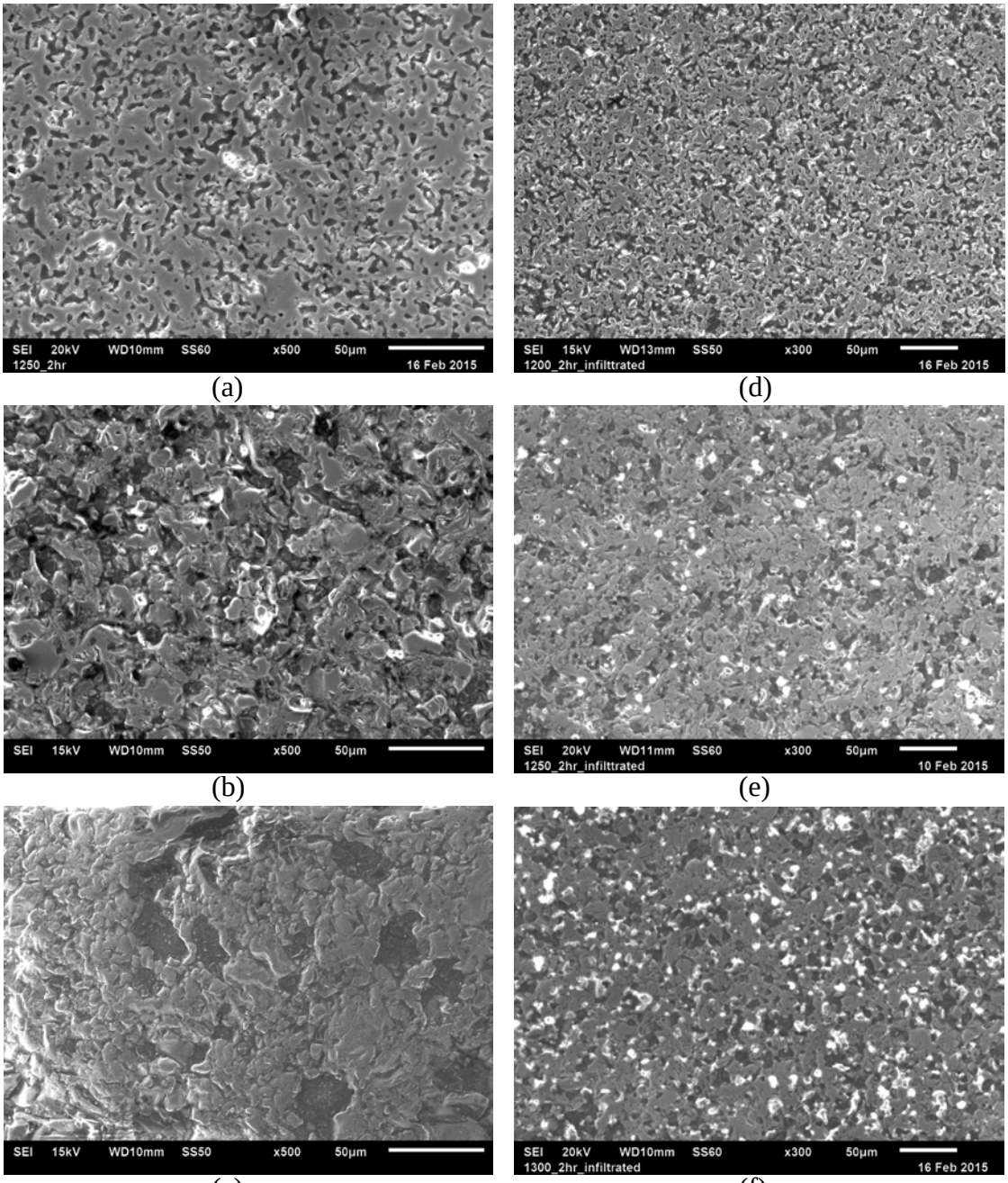

Figure 23: SEM images of the surface of pellets without infiltration sintered for 2 hours at (a)1200°C, (b)1250°C, (c)1300°C and pellets sintered for 2 hours at (d)1200°C without water treated, (e)1250°C without water treated, and (f)1300°C without water treated

5.2.2 XRD analysis

Diffraction patterns of the infiltrated pellets surface showed no obvious evidence for all of the calcium rich phases. Only the diffraction pattern of the pellet sintered at 1300°C is shown below, because the diffraction patterns of the pellets sintered at 1200°C and 1250°C are similar to that of the pellets sintered at 1300°C and results obtained are the same.

Figure 24(a) demonstrates that there are only few peaks of CaO (light blue lines) and they are all overlapped with the peaks of β-TCP, making it very difficult to identify CaO from β-TCP. Figure 24(b) displays that the peak 2θ=33.89° (red line) for $CaCO_3$ is not present at fractions above the detection limit. As is can be seen in Figure 24(c) and figure 24(d), the peak 2θ=33.34° and 2θ=20.82° (green lines) also fail to show up, providing no evidence for $Ca(OH)_2$ .Finally, the formation of HA is not identified according to the absence of the peak at 2θ=37.16° (black lines)as shown in figure 24(e).

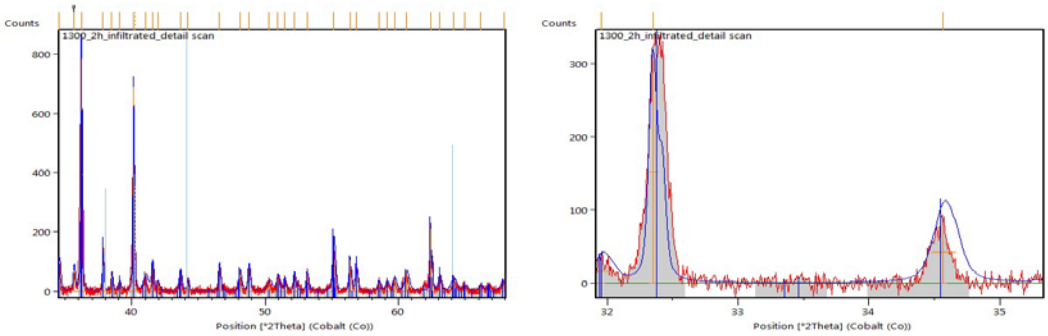

(a)

(b)

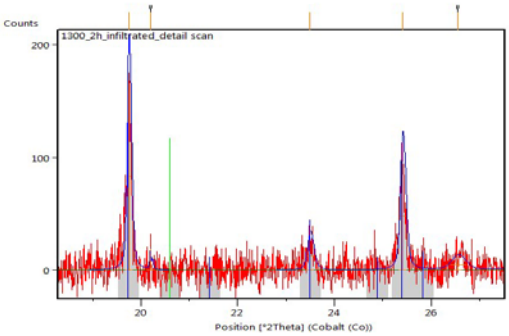

(c)

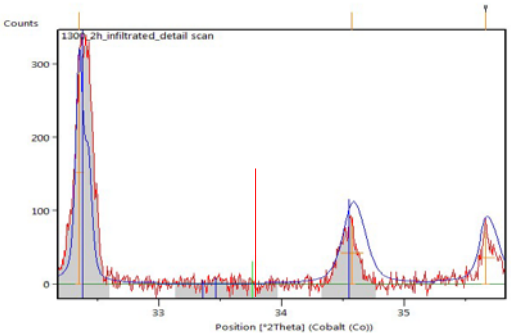

(d)

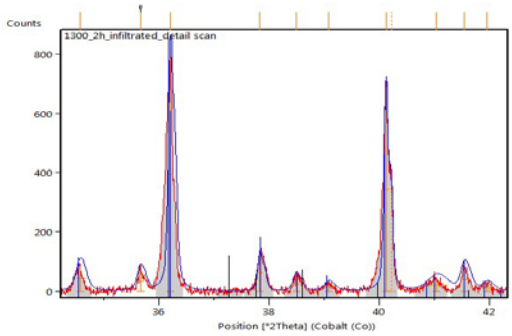

(e)

Figure 24: Amplified images of diffraction patterns of the infiltrated pellets sintered at 1300°C in a specified angle range for (a) CaO, (b) CaCO3 (c) (d)Ca(OH)2, and (e)HA detection

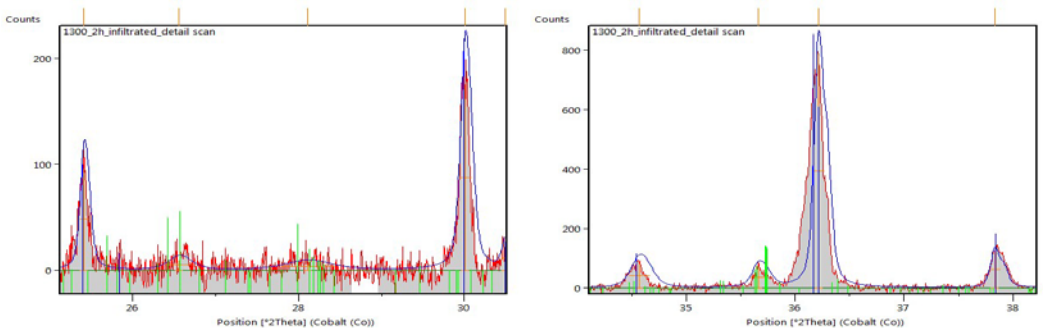

Figure 25: Amplified images of diffraction pattern of infiltrated pellet sintered at 1300°C in a specified angel range to identify α-TCP

Interestingly, the existence of α-TCP was detected according to the diffraction pattern of the infiltrated pellets sintered at 1300°C. As it is demonstrated in figure 25, the main peak of α-TCP ($2\theta=35.8°$, green line) is present and well-distinguished from the peak of β-TCP. Additionally, weaker peaks ranging from $26°<2\theta<29°$ were observed also. The identification of α-TCP was not found in the diffraction patterns of the pellet, which has the same heat treatment but without Ca infiltration. The scan time and scan step size were also the same. The quantity of α-TCP is estimated to be 11% according to the analysis software. This finding suggests that increase the content of calcium might be able to stabilize α-TCP phase or stimulate the transformation from β-TCP to α-TCP.

In the research of Miranda,[188] it is reported that no clear evidence shows the transformation from β-TCP to α-TCP in Ca-deficient β-TCP (ratio of Ca/P<1.5) sintered at 1300°C for 2 hours, which is consistent with the results presented in 5.1. It is also reported by Miranda et al that Ca-rich β-TCP (ratio of Ca/P>1.5) can transform completely to α-TCP at 1500°C for 2 hours suggested the α-phase is stabilized.

Similar to α-TCP in pellets without infiltration, the small amount of the Ca phases introduced by infiltration is one of the barriers to identify them. So, one more detailed XRD scan

was conducted with an even longer scanning time and even more narrowed step size, in order to identify Ca rich phases. The sample used for this scan is the powder ground from the infiltrated pellet sintered at 1300 °C. Since the previous XRD analysis focuses on the surface of the pellets, the diffraction patterns obtained only represent the phase composition on the surface. In contrast, XRD on the powder would result in a diffraction pattern reflecting the average phase composition of the whole pellet. As expected, some of the Ca phases were detected.

Figure 26(a) and (b) demonstrates that the peaks of $Ca(OH)_2$(2θ=33.34°, and 2θ=20.82°, green lines) were found in the diffraction patterns, although the intensity of the peaks is really low. The peak showed in figure 26(b) (green line) also can be an indication of $CaCO_3$, as it is displayed in figure 26(c) (green line), noticing that the peak of $Ca(OH)_2$(2θ=33.34°) is quite close to the peak of $CaCO_3$: (2θ=33.89°). Since the peak at 2θ=20.82° is the main peak of the $Ca(OH)_2$, the intensity of peak at 2θ=20.82° should be higher than the peak at 2θ=33.34° if only $Ca(OH)_2$ exists, which is contrary to the relative intensities of the peaks(green lines) showed in figure 26(a) and (b). Therefore, $Ca(OH)_2$ and $CaCO_3$ are more likely to be co-existing.

Furthermore, no evidence for the existence of HA were found as it is shown in figure 26(d). So it is suggested that the reaction of CaO+TCP=HA were hardly involved in sintering of the infiltrated samples. It is much more likely that Ca went into solution in TCP and stabilized the α-phase leaving only minor amounts of calcium rich phases.

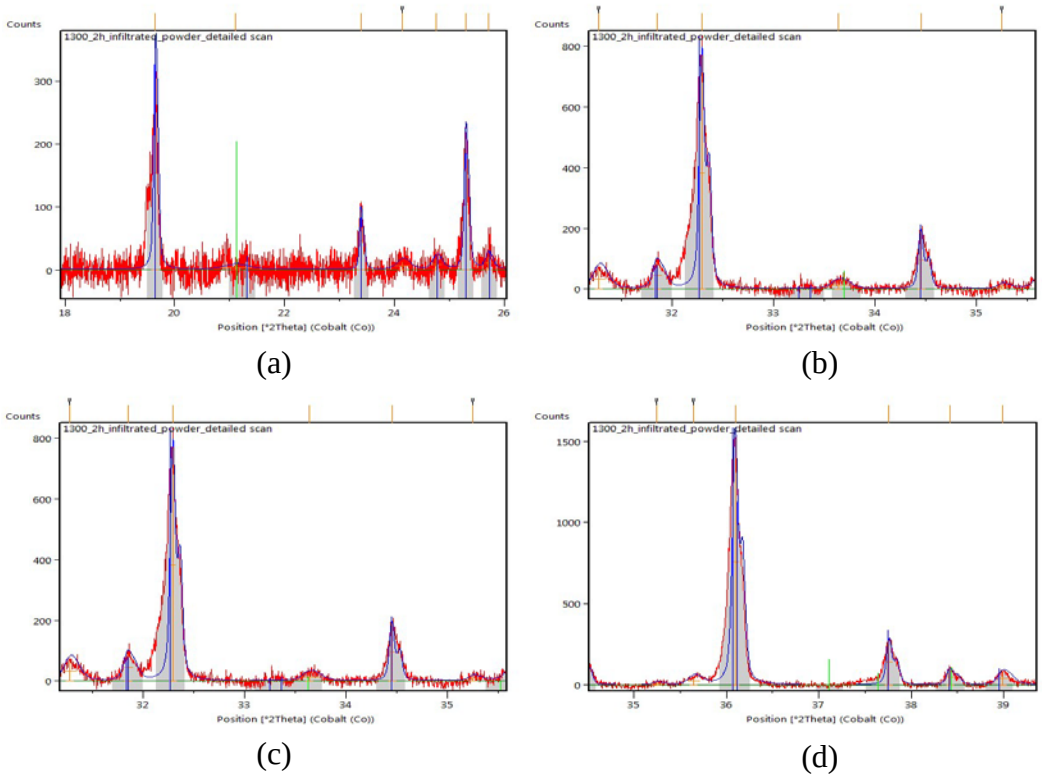

Figure 26: Amplified images of the diffraction pattern of the powder ground from infiltrated pellets sintered at 1300°C

5.3 INFILTRATED FOAMS

TCP foams were processed using an emulsion direct foaming method and some of the foams were partially sintered and infiltrated with different concentration of Ca (0mol/L, 1mol/L, and 2mol/L) in the same way as the pellets. The foams were then immersed in water for different times up to 4 weeks. Figure 27 shows low magnification SEM images of foams with different concentration of infiltrated Ca at different immersion time points. The defects circled on the images of foam with 2mol/L infiltration at time point of 4 weeks (Figure 27(i)) might be the defects caused by the dissolution of introduced Ca rich phase. However, similar defects were

found also in all other foams with or without infiltration, suggesting that there is no significant difference. Also, there is not an effective method to quantify the number of these kinds of defects in each foam because stereological techniques cannot be accurately applied to curved surfaces. Since the defects are quite large and have smooth surfaces so they could have been formed during the foaming processing instead of the dissolution of infiltrated of Ca phase.

Other smaller defects were also found in both in foams with or without infiltration. As is shown in the circle in figure 28. However, they are also found in un-infiltrated pellets and are difficult to quantify, so the hypothesis that Ca rich phases will result from infiltration and preferentially dissolve are not supported by the results of this study. It is more likely that the calcium increases the calcium to phosphorous ratio of the TCP pellets and foams and thereby stabilizes the α-phase.

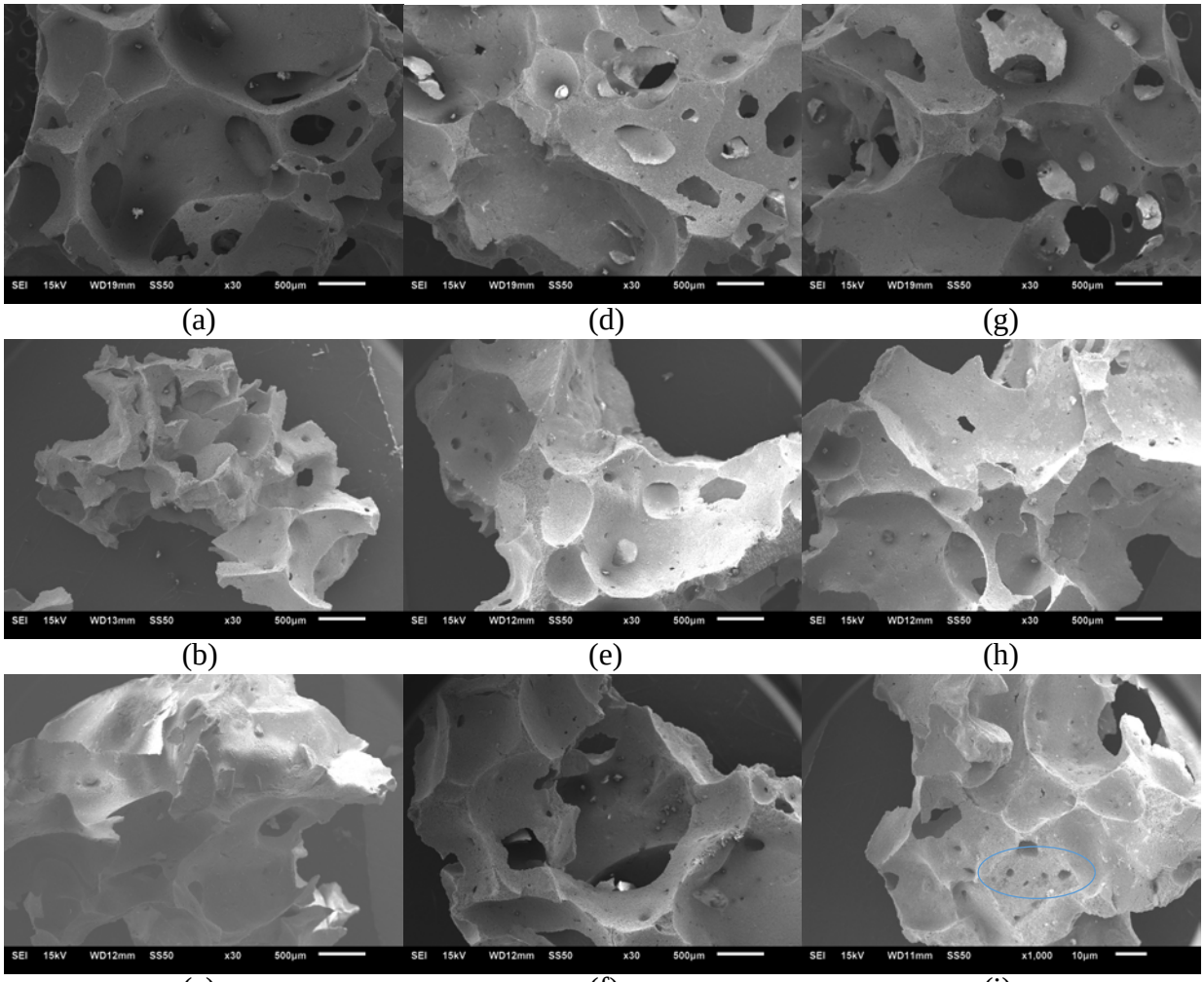

(a) (d) (g)

(b) (e) (h)

(c) (f) (i)

Figure 27: SEM images of foams with 0mol/L Ca infiltrated: (a)0.5 hours, (b)3 days, and (c)29 days; with 1mol/L Ca infiltrated: (d)0.5 hours, (e)3 days, and (f)29 days; with 2mol/L Ca infiltrated: (g)0.5 hours, (h)3 days, and (i)29 days

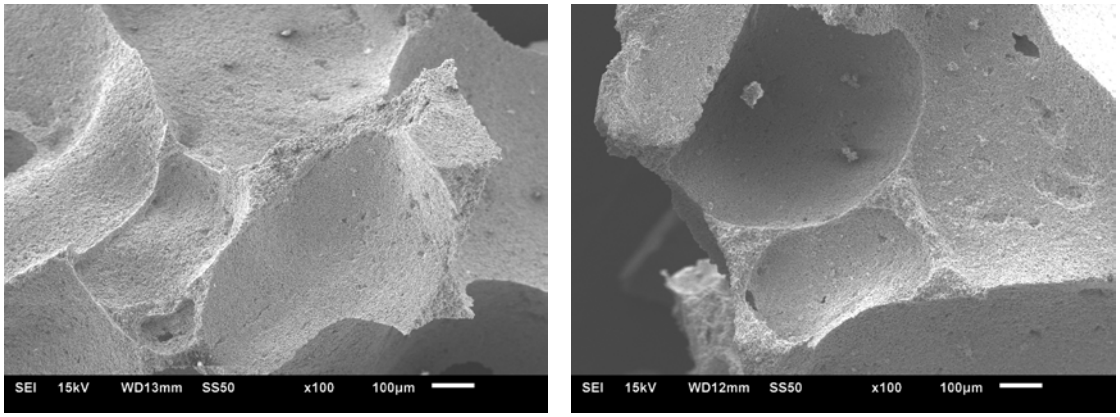

(a) (b)

Figure 28: SEM of images of foams (a)with 0mol/L Ca infiltrated after 3 days immersion, (b)with 2mol/L Ca infiltrated after 3 days immersion

6.0 CONCLUSION

The sintering behavior of β-TCP was investigated and compared with calcium infiltrated samples.

1. β-TCP was unable to reach high sintered density in pellets in the temperature range 1200°C to 1300°C. Microstructural investigation suggest that this was due to coarsening of the microstructure at the higher temperatures that increases the effective diffusion distance for densification. High temperature sintering resulted in evidence of melting that may suggest the β-TCP powder used was calcium deficient.
2. Infiltration of amount up to 2mol/L of calcium rich salts results in the stabilization of α-TCP in pellets sintered at higher temperature rather than the formation of calcium rich phases. Water treatment of the infiltrated samples did produce defects but their origin is unclear. No evidence of hydroxyapatite formation was observed in the sintered samples.
3. β-TCP foams were successfully processed using a emulsion based direct foaming method. Immersion of the foams for times up to 4 weeks showed no evidence of defects produced by preferential dissolution of second phases.

7.0 FUTURE WORK

The following future experiments are recommended

1. Quantitative measurement of the calcium concentration in buffered saline should be measured after exposure to infiltrated foams and un-infiltrated foams over a period of 4 weeks. Additionally, the mechanical properties and fragmentation of the foams should be quantified.
2. Attempts should be made to sinter calcium rich TCP at lower temperature to avoid the coarsening and thereby reach higher density. The effect of other susbstitutional elements on densification should be studied quantitatively

8.0 ACKNOWLEDGEMENT

I would like to express my deepest appreciation to all those who provided me the possibility to complete this report.

A special gratitude I give to my advisor, Dr. Nettleship, whose contribution in stimulating suggestions and encouragement, helped me to coordinate my master thesis

Furthermore I would also like to acknowledge with much appreciation the important role of Qinghao Zhang, who gave the constructive advice to my research and taught me the necessary laboratory skills.

BIBLIOGRAPHY

[1] Terzic, Andre, and Timothy J. Nelson. “Regenerative Medicine.” Journal of the American College of Cardiology 55, no. 20 (May 2010): 2254–57. doi:10.1016/j.jacc.2009.12.050.

[2] Gahrton G, Björkstrand B, ‘Progress in haematopoietic stem cell transplantation for multiple myeloma’. *J Intern Med*, 248 (3): 185–201. (2000).

[3] Gratwohl, A., H. Baldomero, M. Gratwohl, M. Aljurf, L. F. Bouzas, M. Horowitz, Y. Kodera, et al. “Quantitative and Qualitative Differences in Use and Trends of Hematopoietic Stem Cell Transplantation: A Global Observational Study.” *Haematologica* 98, no. 8 (August 1, 2013): 1282–90. doi:10.3324/haematol.2012.076349.

[4] Shlomchik, Warren D. “Graft-versus-Host Disease.” *Nature Reviews Immunology* 7, no. 5 (May 2007): 340–52. doi:10.1038/nri2000.

[5] Remes, Kari, and Allan Rajamäki. “Autologous Stem Cell Transplantations.” *Annals of Medicine* 28, no. 2 (January 1996): 79–82. doi:10.3109/07853899609092929.

[6] Ringe, Jochen, and Michael Sittinger. “Regenerative Medicine: Selecting the Right Biological Scaffold for Tissue Engineering.” *Nature Reviews Rheumatology* 10, no. 7 (May 27, 2014): 388–89. doi:10.1038/nrrheum.2014.79.

[7] El-Ghannam, A. Bone reconstruction: from bioceramics to tissue engineering. Expert Rev Med Devices 2, 87, 2005.

[8] Hench LL, Wilson J. Surface-active biomaterials. Science 1984;226:630–6.

[9] David T. Scadden, ‘The stem-cell niche as an entity of action’, *NATURE*, 441 (7097):1075-9. (2006).

[10] Shinya Nakamura, M.S.,1 Takuya Matsumoto, D.D.S., Ph.D.,2 Jun-Ichi Sasaki, D.D.S.,2 et tl., ‘Effect of Calcium Ion Concentrations on Osteogenic Differentiation and Hematopoietic Stem Cell Niche-Related Protein Expression in Osteoblasts’ , *TISSUE ENGINEERING*: Part A, 16(8):2467-73 ,(2010)

[11] Glotzbach, Jason P., Victor W. Wong, Geoffrey C. Gurtner, and Michael T. Longaker. “Regenerative Medicine.” Current Problems in Surgery 48, no. 3 (March 2011): 148–212. doi:10.1067/j.cpsurg.2010.11.002.

[12] Mason, Chris, and Peter Dunnill. “A Brief Definition of Regenerative Medicine.” Regenerative Medicine 3, no. 1 (January 2008): 1–5. doi:10.2217/17460751.3.1.1.

[13] Maienschein, Jane. “Regenerative Medicine’s Historical Roots in Regeneration, Transplantation, and Translation.” Developmental Biology 358, no. 2 (October 2011): 278–84. doi:10.1016/j.ydbio.2010.06.014.

[14] Mason, Chris, and Peter Dunnill. “A Brief Definition of Regenerative Medicine.” Regenerative Medicine 3, no. 1 (January 2008): 1–5. doi:10.2217/17460751.3.1.1.

[15] TheFreeDictionary.com. S.v. "Cell therapy." Retrieved December 6 2014 from http://encyclopedia.thefreedictionary.com/Cell+Therapy

[16] Gage, FH (1998). "Cell therapy". Nature 392 (6679 Suppl): 18–24.

[17] "Cell Therapy". American Cancer Society. 1 November 2008. Retrieved 15 September 2014.

[18] Nadig, RoopaR. “Stem Cell Therapy - Hype or Hope? A Review.” Journal of Conservative Dentistry 12, no. 4 (2009): 131. doi:10.4103/0972-0707.58329.

[19] "immunotherapies definition". Dictionary.com. Retrieved 2009-06-02

[20] Koh, Mickey B.C., and Garnet Suck. “Cell Therapy: Promise Fulfilled?” Biologicals 40, no. 3 (May 2012): 214–17. doi:10.1016/j.biologicals.2011.12.002.

[21] Gene Therapy and Cell Therapy Defined. American society of Gene and Cell Therapy. http://www.asgct.org/general-public/educational-resources/gene-therapy--and-cell-therapy-defined. Retrieved 15 September 2014

[22] Parish, CL; Arenas, E (2007). "Stem-cell-based strategies for the treatment of Parkinson's disease". Neuro-degenerative diseases 4 (4): 339–47.

[23] Wysoczynski, Marcin, Kyung U Hong, and Joseph B Moore. “Bone Marrow Cell Therapies in Ischemic Cardiomyopathy.” Expert Opinion on Biological Therapy 14, no. 9 (September 2014): 1229–32. doi:10.1517/14712598.2014.925873.

[24] Sanberg, Cyndy Davis., and Paul R. Sanberg. Cell Therapy, Stem Cells, and Brain Repair. Totowa, N.J.: Humana Press, 2006. http://public.eblib.com/choice/publicfullrecord.aspx?p=337722_0.

[25] Dib, Nabil., Doris A. Taylor, and Edward B. Diethrich. Stem Cell Therapy and Tissue Engineering for Cardiovascular Repair from Basic Research to Clinical Applications. New York, NY: Springer, 2006. http://public.eblib.com/choice/publicfullrecord.aspx?p=264909.

[26] Mason, Chris, David A Brindley, Emily J Culme-Seymour, and Natasha L Davie. “Cell Therapy Industry: Billion Dollar Global Business with Unlimited Potential.” Regenerative Medicine 6, no. 3 (May 2011): 265–72. doi:10.2217/rme.11.28.

[27] Langer, R., and J. P. Vacanti. “Tissue Engineering.” Science (New York, N.Y.) 260, no. 5110 (May 14, 1993): 920–26.

[28] National Science Foundation (U.S.A.) (2004). "The Emergence of Tissue Engineering as a Research Field". Retrieved 28 September

2014.

[29] Bianco, Paolo, and Pamela Gehron Robey. “Stem Cells in Tissue Engineering.” Nature 414, no. 6859 (2001): 118–21.

[30] Mikos, Antonios G., and Johnna S. Temenoff. “Formation of Highly Porous Biodegradable Scaffolds for Tissue Engineering.” Electronic Journal of Biotechnology 3, no. 2 (2000): 23–24.

[31] Marolt, Darja, Miomir Knezevic, and Gordana Vunjak Novakovic. “Bone Tissue Engineering with Human Stem Cells.” Stem Cell Res Ther 1, no. 10 (2010): 20637059.

[32] "Creating artificial bone marrow". The Economist. 7 January 2009.

[33] Stevens, Molly M. “Biomaterials for Bone Tissue Engineering.” Materials Today 11, no. 5 (May 2008): 18–25. doi:10.1016/S1369-7021(08)70086-5.

[34] Olszta, Matthew J., Xingguo Cheng, Sang Soo Jee, Rajendra Kumar, Yi-Yeoun Kim, Michael J. Kaufman, Elliot P. Douglas, and Laurie B. Gower. “Bone Structure and Formation: A New Perspective.” Materials Science and Engineering: R: Reports 58, no. 3–5 (November 2007): 77–116. doi:10.1016/j.mser.2007.05.001.

[35] Reznikov, Natalie, Ron Shahar, and Steve Weiner. “Bone Hierarchical Structure in Three Dimensions.” Acta Biomaterialia 10, no. 9 (September 2014): 3815–26. doi:10.1016/j.actbio.2014.05.024.

[36] Currey, John D.. Bones : Structure and Mechanics. Princeton, NJ, USA: Princeton University Press, 2013. Accessed December 6, 2014. ProQuest ebrary.

[37] http://upload.wikimedia.org/wikipedia/commons/1/12/Bone_cross-section.svg

[38] Woodburne, Russell Thomas. Musculoskeletal System Part 1, Part 1,. Summit N.J.: Ciba-Geigy Corp., 1987.

[39] Hall, Susan. Basic Biomechanics. Fifth Edition: 88. (2007)

[40] Netter, Frank H.; Dingle, Regina V.; Mankin, Henry J. (1990). *Musculoskeletal system: anatomy, physiology, and metabolic disorders*. Summit, New Jersey: Ciba-Geigy Corporation. p. 170.

[41] Young, Barbara, ed. Wheater's Functional Histology: A Text and Colour Atlas. 5th ed. Edinburgh? Churchill Livingstone/Elsevier, 2006.

[42] Hall, Susan J. Basic Biomechanics. Boston, Mass.: McGraw-Hill, 2007.

[43] Gomez, Santiago. "Crisóstomo Martinez, 1638-1694: The Discoverer of Trabecular Bone." Endocrine 17, no. 1 (February 2002): 3–4. doi:10.1385/ENDO:17:1:03.

[44] Nalla, R.K., J.J. Kruzic, J.H. Kinney, and R.O. Ritchie. "Effect of Aging on the Toughness of Human Cortical Bone: Evaluation by R-Curves." *Bone* 35, no. 6 (December 2004): 1240–46. doi:10.1016/j.bone.2004.07.016.

[45] Netter, Frank H.; Dingle, Regina V.; Mankin, Henry J. (1990). *Musculoskeletal system: anatomy, physiology, and metabolic disorders*. Summit, New Jersey: Ciba-Geigy Corporation. p. 170.

[46] http://en.wikipedia.org/wiki/Bone_marrow#cite_ref-1

[47] Stites, D. P., M. D., A. I., M. D. Terr, and T. G., M. D. PhD. Parslow. Medical Immunology. Stamford: Lange Medical Publishers, 1997.

[48] Vunjak-Novakovic, Gordana, Nina Tandon, Amandine Godier, Robert Maidhof, Anna Marsano, Timothy P. Martens, and Milica Radisic. "Challenges in Cardiac Tissue Engineering." Tissue Engineering Part B: Reviews 16, no. 2 (April 2010): 169–87. doi:10.1089/ten.teb.2009.0352.

[49] Morrison, J.; Judith Kimble (2006). "Asymmetric and symmetric stem-cell divisions in development and cancer". Nature 441 (7097): 1068–74.

[50] Morrison, J.; Judith Kimble. 1) Asymmetric and symmetric stem-cell divisions in development and cancer.

[51] Raphael Rubin and David S. Strayer (2007). Rubin's Pathology: Clinicopathologic Foundations of Medicine. Lippincott Williams & Wilkins. p. 90.

[52] Bladé J, Samson D, Reece D, et al. (1998). "Criteria for evaluating disease response and progression in patients with multiple myeloma treated by high-dose therapy and haemopoietic stem cell transplantation. Myeloma Subcommittee of the EBMT. European Group for Blood and Marrow Transplant". Br. J. Haematol. 102 (5): 1115–23.

[53] Pavletic SZ, Khouri IF, Haagenson M, et al. (2005). "Unrelated donor marrow transplantation for B-cell chronic lymphocytic leukemia after using myeloablative conditioning: results from the Center for International Blood and Marrow Transplant research". J. Clin. Oncol. 23 (24): 5788–94

[54] " Hematopoietic Stem Cells." Stem Cell Information. National Institutes of Health, U.S. Department of Health and Human Services, 17 Jun 2011. Web. 9 Nov 2013.

[55] Marolt, Darja, Miomir Knezevic, and Gordana Vunjak Novakovic. "Bone Tissue Engineering with Human Stem Cells." Stem Cell Res Ther 1, no. 10 (2010): 20637059.

[56] Nardi, N. Beyer; da Silva Meirelles, L. (2006). "Mesenchymal Stem Cells: Isolation, In Vitro Expansion and Characterization". In Wobus, Anna M.; Boheler, Kenneth. Stem Cells. Handbook of experimental pharmacology 174. pp. 249–82.

[57] Caplan, Arnold I. "Adult Mesenchymal Stem Cells for Tissue Engineering versus Regenerative Medicine." Journal of Cellular Physiology 213, no. 2 (November 2007): 341–47. doi:10.1002/jcp.21200.

[58] Gale Encyclopedia of Medicine. S.v. "Human Leukocyte Antigen Test." Retrieved December 7 2014
from http://medical-dictionary.thefreedictionary.com/Human+Leukocyte+Antigen+Test

[59] Graft-versus-host disease. Medline Plus. Retrieved 12, Oct, 2014. http://www.nlm.nih.gov/medlineplus/ency/article/001309.htm

[60] Canellos, George (1997). "The Role of Salvage Therapy in Malignant Lymphomas". The Oncologist 2 (3): 181–183.

[61] Stamm, Christof, Bernd Westphal, Hans-Dieter Kleine, Michael Petzsch, Christian Kittner, Heiko Klinge, Carl Schümichen, Christoph A Nienaber, Mathias Freund, and Gustav Steinhoff. "Autologous Bone-Marrow Stem-Cell Transplantation for Myocardial Regeneration." The Lancet 361, no. 9351 (January 2003): 45–46. doi:10.1016/S0140-6736(03)12110-1.

[62] Lee, Jin Soo, Ji Man Hong, Gyeong Joon Moon, Phil Hyu Lee, Young Hwan Ahn, and Oh Young Bang. "A Long-Term Follow-Up Study of Intravenous Autologous Mesenchymal Stem Cell Transplantation in Patients With Ischemic Stroke." STEM CELLS 28, no. 6 (April 19, 2010): 1099–1106. doi:10.1002/stem.430.

[63] Moreau, P., H. Avet-Loiseau, J.-L. Harousseau, and M. Attal. “Current Trends in Autologous Stem-Cell Transplantation for Myeloma in the Era of Novel Therapies.” Journal of Clinical Oncology 29, no. 14 (May 10, 2011): 1898–1906. doi:10.1200/JCO.2010.32.5878.

[64] Couri C et al. (2009). "C-peptide levels and insulin independence following autologous nonmyeloablative hematopoietic stem cell transplantation in newly diagnosed type 1 diabetes mellitus". JAMA 301 (15): 1573–1579.

[65] Kersey, John H., Daniel Weisdorf, Mark E. Nesbit, Tucker W. LeBien, William G. Woods, Philip B. McGlave, Tae Kim, et al. “Comparison of Autologous and Allogeneic Bone Marrow Transplantation for Treatment of High-Risk Refractory Acute Lymphoblastic Leukemia.” New England Journal of Medicine 317, no. 8 (August 20, 1987): 461–67. doi:10.1056/NEJM198708203170801.

[66] Bruno, Benedetto, Marcello Rotta, Francesca Patriarca, Nicola Mordini, Bernardino Allione, Fabrizio Carnevale-Schianca, Luisa Giaccone, et al. “A Comparison of Allografting with Autografting for Newly Diagnosed Myeloma.” New England Journal of Medicine 356, no. 11 (March 15, 2007): 1110–20. doi:10.1056/NEJMoa065464.

[67] Nigel Russell, Eric Bessell, Claire. “Allogeneic Haemopoietic Stem Cell Transplantation for Multiple Myeloma or Plasma Cell Leukaemia Using Fractionated Total Body Radiation and High-Dose Melphalan Conditioning.” Acta Oncologica 39, no. 7 (January 2000): 837–41. doi:10.1080/028418600750063596.

[68] Khang, Gilson. *Handbook of Intelligent Scaffolds for Tissue Engineering and Regenerative Medicine*. Boca Raton: CRC Press, 2012. http://site.ebrary.com/id/10535469.

[69] O’Brien, Fergal J. “Biomaterials & Scaffolds for Tissue Engineering.” *Materials Today* 14, no. 3 (March 2011): 88–95. doi:10.1016/S1369-7021(11)70058-X.

[70] M. V. Risbud and M. Sittinger, “Tissue engineering: advances in in vitro cartilage generation,” *Trends in Biotechnology*, vol. 20, no. 8, pp. 351–356, 2002.

[71]Yusop, A. H., A. A. Bakir, N. A. Shaharom, M. R. Abdul Kadir, and H. Hermawan. “Porous Biodegradable Metals for Hard Tissue Scaffolds: A Review.” *International Journal of Biomaterials* 2012 (2012): 1–10. doi:10.1155/2012/641430.

[72] Hing, Karin A. “Bioceramic Bone Graft Substitutes: Influence of Porosity and Chemistry.” *International Journal of Applied Ceramic Technology* 2, no. 3 (2005): 184–99.

[73] Muschler, George F., Chizu Nakamoto, and Linda G. Griffith. “Engineering Principles of Clinical Cell-Based Tissue Engineering.” *The Journal of Bone & Joint Surgery* 86, no. 7 (2004): 1541–58.

[74] Nguyen, Lonnissa H., Nasim Annabi, Mehdi Nikkhah, Hojae Bae, Loïc Binan, Sangwon Park, Yunqing Kang, Yunzhi Yang, and Ali Khademhosseini. “Vascularized Bone Tissue Engineering: Approaches for Potential Improvement.” *Tissue Engineering Part B: Reviews* 18, no. 5 (October 2012): 363–82. doi:10.1089/ten.teb.2012.0012.

[75] Zhang, P., Hamamura, K., and Yokota, H. A brief review of bone adaptation to unloading. J Proteomics Bioinform 6, 4, 2008.

[76] Cordonnier, T., Sohier, J., Rosset, P., and Layrolle, P. Bio- mimetic materials for bone tissue engineering—state of the art and future trends. Adv Biomater 13, B135, 2011

77 Bertazzo, S. & Bertran, C. A. "Morphological and dimensional characteristics of bone mineral crystals". *Bioceramics*. 309–311 (Pt. 1, 2): 3–10. (2006).

[78] El-Ghannam, A. Bone reconstruction: from bioceramics to tissue engineering. Expert Rev Med Devices 2, 87, 2005.

[79] Cordonnier, T., Sohier, J., Rosset, P., and Layrolle, P. Bio- mimetic materials for bone tissue engineering—state of the art and future trends. Adv Biomater 13, B135, 2011.

[80] Rezwan, K., Chen, Q.Z., Blaker, J.J., and Boccaccini, A.R. Biodegradable and bioactive porous polymer/inorganic composite scaffolds for bone tissue engineering. Biomaterials 27, 3413, 2006.

[81] Kanazawa T, editor. Inorganic phosphate materials. Kindlington, Oxford: Elsevier Science, 1989. p. 30.

[82] John W. Anthony, Richard A. Bideaux, Kenneth W. Bladh, and Monte C. Nichols, Eds., Handbook of Mineralogy, Mineralogical Society of America, Chantilly, VA 20151-1110, USA. http://www.handbookofmineralogy.org/.

[83] Brunton, P. A., R. P. W. Davies, J. L. Burke, A. Smith, A. Aggeli, S. J. Brookes, and J. Kirkham. “Treatment of Early Caries Lesions Using Biomimetic Self-Assembling Peptides – a Clinical Safety Trial.” *BDJ* 215, no. 4 (August 23, 2013): E6–E6. doi:10.1038/sj.bdj.2013.741.

[84] Junqueira, Luiz Carlos; José Carneiro (2003). Foltin, Janet; Lebowitz, Harriet; Boyle, Peter J., eds. *Basic Histology, Text & Atlas* (10th ed.). McGraw-Hill Companies. p. 144

[85] http://en.wikipedia.org/wiki/Hydroxylapatite#cite_note-4

[86] What Is Calcium Phosphate?. LIVESTRONG.COM. Retrieved 30, Oct, 2014. http://www.livestrong.com/article/475373-what-is-calcium-phosphate/

[87] Dorozhkin, Sergey V. “Biphasic, Triphasic and Multiphasic Calcium Orthophosphates.” *Acta Biomaterialia* 8, no. 3 (March 2012): 963–77. doi:10.1016/j.actbio.2011.09.003.

[88] Nguyen, Lonnissa H., Nasim Annabi, Mehdi Nikkhah, Hojae Bae, Loïc Binan, Sangwon Park, Yunqing Kang, Yunzhi Yang, and Ali Khademhosseini. “Vascularized Bone Tissue Engineering: Approaches for Potential Improvement.” *Tissue Engineering Part B: Reviews* 18, no. 5 (October 2012): 363–82. doi:10.1089/ten.teb.2012.0012.

[89] Yashima, Masatomo, Atsushi Sakai, Takashi Kamiyama, and Akinori Hoshikawa. “Crystal Structure Analysis of B-Tricalcium Phosphate $Ca_3(PO4)_2$ by Neutron Powder Diffraction.” *Journal of Solid State Chemistry* 175, no. 2 (November 2003): 272–77. doi:10.1016/S0022-4596(03)00279-2.

[90] http://en.wikipedia.org/wiki/Tricalcium_phosphate

[91] Yoichi Kawaike, Masatomo Yashima, Masahiko Tanaka. “crystal structure of tricalcium phosphate”. National Institute for Materials Science, Japan.

[92] Carrodeguas, R.G., and S. De Aza. “A-Tricalcium Phosphate: Synthesis, Properties and Biomedical Applications.” *Acta Biomaterialia* 7, no. 10 (October 2011): 3536–46. doi:10.1016/j.actbio.2011.06.019.

[93] M. Bohner. Calcium orthophosphates in medicine: from ceramics to calcium phosphate cements. Injury, 31 (Suppl. D) (2000), pp. 37–47.

[94] S.V. Dorozhkin. Calcium orthophosphate cements for biomedical application. J Mater Sci, 43 (2008), pp. 3028–3057.

[95] David T. Scadden, ‘The stem-cell niche as an entity of action’, *NATURE*, 441 (7097):1075-9. (2006).

[96] Shinya Nakamura, M.S.,1 Takuya Matsumoto, D.D.S., Ph.D.,2 Jun-Ichi Sasaki, D.D.S.,2 et tl., ‘Effect of Calcium Ion Concentrations on Osteogenic Differentiation and Hematopoietic Stem Cell Niche-Related Protein Expression in Osteoblasts’ , *TISSUE ENGINEERING*: Part A, 16(8):2467-73 ,(2010)

[97] M.T. Fulmer, I.C. Ison, C.R. Hankermayer, B.R. Constantz, J. Ross, Measurements of the solubilities and dissolution rates of several hydroxyapatite. Biomaterials 23, 751–755 (2002)

[98] Yang, H. Y., I. Thompson, S. F. Yang, X. P. Chi, J. R. G. Evans, and R. J. Cook. “Dissolution Characteristics of Extrusion Freeformed Hydroxyapatite–tricalcium Phosphate

Scaffolds." *Journal of Materials Science: Materials in Medicine* 19, no. 11 (November 2008): 3345–53. doi:10.1007/s10856-008-3473-7.

[99] F. Fazan, P.M. Marquis, Dissolution behavior of plasma-sprayed hydroxyapatite coatings. J. Mater. Sci.: Mater. Med. 11, 782–792 (2000)

[100] Bohner, M. "Calcium Orthophosphates in Medicine: From Ceramics to Calcium Phosphate Cements." *Injury* 31 (2000): D37–47.

[101] L.C. Chow. Development of self-setting calcium phosphate cements. J Ceram Soc Jpn, 99 (10) (1991), pp. 954–964.

[102] Junqueira, Luiz Carlos; José Carneiro (2003). Foltin, Janet; Lebowitz, Harriet; Boyle, Peter J., eds. *Basic Histology, Text & Atlas* (10th ed.). McGraw-Hill Companies. p. 144

[103] Vert, Michel, Yoshiharu Doi, Karl-Heinz Hellwich, Michael Hess, Philip Hodge, Przemyslaw Kubisa, Marguerite Rinaudo, and François Schué. "Terminology for Biorelated Polymers and Applications (IUPAC Recommendations 2012)." *Pure and Applied Chemistry* 84, no. 2 (January 11, 2012). doi:10.1351/PAC-REC-10-12-04.

[104] Atala, Anthony, and R. P. Lanza, eds. *Methods of Tissue Engineering*. San Diego, CA: Academic Press, 2001.

[105] Burdick, Jason A., and Robert L. Mauck, eds. *Biomaterials for Tissue Engineering Applications: A Review of the Past and Future Trends*. Wien [Austria] ; p191. New York: Springer, 2011.

[106] Gallinetti, Sara, Cristina Canal, and Maria-Pau Ginebra. "Development and Characterization of Biphasic Hydroxyapatite/β-TCP Cements." Edited by J. Ferreira. *Journal of the American Ceramic Society* 97, no. 4 (April 2014): 1065–73. doi:10.1111/jace.12861.

[107] Shi, Donglu, ed. *Biomaterials and Tissue Engineering*. 1st ed. Biological and Medical Physics, Biomedical Engineering. Berlin ; New York: Springer-Verlag Berlin Heidelberg, 2004.

[108] . Z. Chen, A. R. Boccaccini, H. B. Zhang, D. Z. Wang, and M. J. Edirisinghe, "Improved Mechanical Reliability of Bone Tissue Engineering (Zirconia) Scaffolds by Electrospraying," J. Am. Ceram. Soc., 89 [5] 1534–9 (2006).

[109] Q. Z. Chen, I. D. Thompson, and A. R. Boccaccini, "45S5 Bioglass (R)- Derived Glass-Ceramic Scaffolds for Bone Tissue Engineering," Biomaterials, 27 [11] 2414–25 (2006).

[110] Rahaman, Mohamed N., Delbert E. Day, B. Sonny Bal, Qiang Fu, Steven B. Jung, Lynda F. Bonewald, and Antoni P. Tomsia. "Bioactive Glass in Tissue Engineering." *Acta Biomaterialia* 7, no. 6 (June 2011): 2355–73. doi:10.1016/j.actbio.2011.03.016.

[111] Rahaman, Mohamed N., Delbert E. Day, B. Sonny Bal, Qiang Fu, Steven B. Jung, Lynda F. Bonewald, and Antoni P. Tomsia. “Bioactive Glass in Tissue Engineering.” *Acta Biomaterialia* 7, no. 6 (June 2011): 2355–73. doi:10.1016/j.actbio.2011.03.016.

[112] Martin RB, Chapman MW, Sharkey NA, Zissimos SL, Bay B, Shors EC. Bone ingrowth and mechanical properties of coralline hydroxyapatite 1 year after implantation. Biomaterials 1993;14:341–8.

[113] Daculsi G, Laboux O, Malard O, Weiss P. Current state of the art of biphasic calcium phosphate bioceramics. J Mater Sci Mater Med 2003;14:195–200.

[114] ohanizadeh R, Padrines M, Bouler JM, Couchourel D, Fortun Y, Daculsi G. Apatite precipitation after incubation of biphasic calcium-phosphate ceramic in various solutions: influence of seed species and proteins. J Biomed Mater Res 1998;42:530–9.

[115] Daculsi G, Layrolle P. Osteoinductive properties of micro macroporous biphasic calcium phosphate bioceramics. Key Eng Mater 2004;254– 256:1005–8.

[116] Athanasiou KA, Zhu C, Lanctot DR, Agrawal CM, Wang X. Fundamentals of biomechanics in tissue engineering of bone. Tissue Eng. 2000;6(4):361–381.

[117] Isikli, C., V. Hasirci, and N. Hasirci. “Development of Porous Chitosan-Gelatin/hydroxyapatite Composite Scaffolds for Hard Tissue-Engineering Applications.” *Journal of Tissue Engineering and Regenerative Medicine* 6, no. 2 (February 2012): 135–43. doi:10.1002/term.406.

[118] Wei G, Ma PX. Structure and properties of nano-hydroxyapatite/polymer composite scaffolds for bone tissue engineering. Biomaterials. 2004;25(19):4749–4757.

[119] Kim SS, Park MS, Gwak SJ, Choi CY, Kim BS. Accelerated bonelike apatite growth on porous polymer/ ceramic composite scaffolds in vitro. Tissue Eng. 2006;12(10):2997–3006.

[120] Rodrigues CV, Serricella P, Linhares AB, Guerdes RM, Borojevic R, Rossi MA, et al. Characterization of a bovine collagen-hydroxyapatite composite scaffold for bone tissue engineering. Biomaterials. 2003;24(27):4987–4997.

[121] Xue W, et al. Polycaprolactone coated porous tricalcium phosphate scaffolds for controlled release of protein for tissue engineering. Journal of Biomedical Materials Research Part B: Applied Biomaterials. 2009;91B:831–838.

[122] Cao H, Kuboyama N. A biodegradable porous composite scaffold of PGA/β-TCP for bone tissue engineering. Bone. 2010;46:386–395.

[123] Studart, Andre R., Urs T. Gonzenbach, Elena Tervoort, and Ludwig J. Gauckler. “Processing Routes to Macroporous Ceramics: A Review.” *Journal of the American Ceramic Society* 89, no. 6 (June 2006): 1771–89. doi:10.1111/j.1551-2916.2006.01044.x.

[124] KubokiY,TakitaH,KobayashiD,TsurugaE,InoueM, MurataM, etal.BMP-induced osteogenesis on the surface of hydroxyapatite with geometrically feasible and nonfeasible structures:topologyofosteogenesis.JBiomedMaterRes 1998;39(2):190–9.

[125] Story BJ, Wagner WR, Gaisser DM, Cook SD, Rust-Dawicki AM. In vivo performance of a modified CSTi dental implant coating. Int J Oral Maxillofac Implants 1998;13(6):749–57.

[126] . Haber, ‘‘Manual on Catalyst Characterization,’’ Pure Appl. Chem., 63, 1227– 46 (1991).

[127] Hulbert SF, Young FA, Mathews RS, Klawitter JJ, Talbert CD, Stelling FH. Potential of ceramic materials as permanently implantableskeletalprostheses.JBiomedMaterRes1970; 4(3):433–56.

[128] Hing, Karin A. “Bioceramic Bone Graft Substitutes: Influence of Porosity and Chemistry.” *International Journal of Applied Ceramic Technology* 2, no. 3 (2005): 184–99.

[129] Karageorgiou, V, and D Kaplan. “Porosity of 3D Biomaterial Scaffolds and Osteogenesis.” *Biomaterials* 26, no. 27 (September 2005): 5474–91. doi:10.1016/j.biomaterials.2005.02.002.

[130] . Y. Shan, J. F. Yang, J. Q. Gao, W. H. Zhang, Z. H. Jin, R. Janssen, and T. Ohji, ‘‘Porous Silicon Nitride Ceramics Prepared by Reduction–Nitridation of Silica,’’ J. Am. Ceram. Soc., 88 [9] 2594–6 (2005).

[131] I. H. Arita, V. M. Castano, and D. S. Wilkinson, ‘‘Synthesis and Processing of Hydroxyapatite Ceramic Tapes with Controlled Porosity,’’ J. Mater. Sci.—Mater. Med., 6 [1] 19–23 (1995).

[132] Ohji, T, and M Fukushima. “Macro-Porous Ceramics: Processing and Properties.” *International Materials Reviews* 57, no. 2 (March 2012): 115–31. doi:10.1179/1743280411Y.0000000006.

[133] Studart, Andre R., Urs T. Gonzenbach, Elena Tervoort, and Ludwig J. Gauckler. “Processing Routes to Macroporous Ceramics: A Review.” *Journal of the American Ceramic Society* 89, no. 6 (June 2006): 1771–89. doi:10.1111/j.1551-2916.2006.01044.x.

[134] Colombo, Paolo, Cekdar Vakifahmetoglu, and Stefano Costacurta. “Fabrication of Ceramic Components with Hierarchical Porosity.” *Journal of Materials Science* 45, no. 20 (October 2010): 5425–55. doi:10.1007/s10853-010-4708-9.

[135] Wei G, Ma PX. Structure and properties of nano-hydroxyapatite/polymer composite scaffolds for bone tissue engineering. Biomaterials. 2004;25(19):4749–4757.

[136] H.X. Peng, Z. Fan and J.R.G. Evans, "Microstructure of Ceramic Foams", *J. Eur. Ceram. Soc.*, 20 807-813 (2000).

[137] T. Ota, M. Takahashi, T. Hibi, M. Ozawa, S. Suzuki, Y. Hikichi, and H. Suzuki, ''Biomimetic Process for Producing SiC ''Wood'','' J. Am. Ceram. Soc., 78 [12] 3409–11 (1995).

[138] D. M. Roy and S. K. Linnehan, ''Hydroxyapatite Formed from Coral Skeletal Carbonate by Hydrothermal Exchange,'' Nature, 247 [5438] 220–2 (1974).

[139] F. F. Lange and K. T. Miller, ''Open-Cell, Low-Density Ceramics Fabricated from Reticulated Polymer Substrates,'' Adv. Ceram. Mater., 2 [4] 827–31 (1987).

[140] L. MontanaroCorresponding Y. Jorandb, G. Fantozzib, A. Negroa, 'Ceramic foams by powder processing', Journal of the European Ceramic Society, 18,(9): 1339–1350,(1998)

[141] P. Sepulveda, ''Gelcasting Foams for Porous Ceramics,'' Am. Ceram. Soc. Bull., 76 [10] 61–5 (1997).

[142] Isikli, C., V. Hasirci, and N. Hasirci. "Development of Porous Chitosan-Gelatin/hydroxyapatite Composite Scaffolds for Hard Tissue-Engineering Applications." *Journal of Tissue Engineering and Regenerative Medicine* 6, no. 2 (February 2012): 135–43. doi:10.1002/term.406.

[143] P. Colombo, E. Bernardo and L. Biasetto: J. Am. Ceram. Soc., 2004, 87, (1), 152–154.

[144] S. Ding, S. Zhu, Y.-P. Zeng and D. Jiang: J. Eur. Ceram. Soc., 2007, 27, 2095–2102.

[145] J. Luyten, S. Mullens, J. Cooymans, A. M. De Wilde and I. Thijs: Adv. Eng. Mater., 2003, 5, (10), 715–718.

[146] P. Colombo, E. Bernardo, and L. Biasetto, ''Novel Microcellular Ceramics from a Silicone Resin,'' J. Am. Ceram. Soc., 87 [1] 152–4 (2004).

[147] Y. Hotta, P. C. A. Alberius, and L. Bergstrom, ''Coated Polystyrene Particles as Templates for Ordered Macroporous Silica Structures with Controlled Wall Thickness,'' J. Mater. Chem., 13 [3] 496–501 (2003).

[148] T. J. Fitzgerald, V. J. Michaud, and A. Mortensen, ''Processing of Micro- cellular Sic Foams. 2. Ceramic Foam Production,'' J. Mater. Sci., 30 [4] 1037–45 (1995).

[149] N. Miyagawa and N. Shinohara, ‘‘Fabrication of Porous Alumina Ceramics with Uni-Directionally-Arranged Continuous Pores Using a Magnetic Field,’’ J. Ceram. Soc. Jpn., 107 [7] 673–7 (1999).

[150] S. Barg, C. Soltmann, M. Andrade, D. Koch and G. Grathwohl: J. Am. Ceram. Soc., 2008, 91, (9), 2823–2829.

[151] Y.-W. Kim, S.-H. Kim, C. Wang and C. B. Park: J. Am. Ceram. Soc., 2003, 86, 2231–2233.

[152] J. Zeschky, F. Goetz-Neunhoeffer, J. Neubauer, S. H. J. Lo, B. Kummer, M. Scheffler, and P. Greil, ‘‘Preceramic Polymer Derived Cellular Ceramics,’’ Com- posites Sci. Technol., 63 [16] 2361–70 (2003).

[153] Butt, Hans-Jürgen; Graf, Karlheinz; Kappl, Michael (2006). "Physics and Chemistry of Interfaces". p. 9.

[154] Z. P. Du, M. P. Bilbao-Montoya, B. P. Binks, E. Dickinson, R. Ettelaie and B. S. Murray: Langmuir, 2003, 19, (8), 3106–3108.

[155] A. R. Studart, U. T. Gonzenbach, I. Akartuna, E. Tervoort and L. J. Gauckler: J. Mater. Chem., 2007, 17, 3283–3289.

[156] U. T. Gonzenbach, A. R. Studart, E. Tervoort, and L. J. Gauckler, ‘‘Ultra- stable particle-stabilized foams,’’ Angewandte Chemie—Int. Ed., (2006), in press. S. U. Pickering, ‘‘Emulsions,’’ J. Chem. Soc., 91, 2001–21 (1907).

[157] Champion, E. “Sintering of Calcium Phosphate Bioceramics.” *Acta Biomaterialia* 9, no. 4 (April 2013): 5855–75. doi:10.1016/j.actbio.2012.11.029.

[158] Kleebe HJ, Bres EF, Bernache-Assollant D, Ziegler G. High-resolution electron microscopy and convergent beam electron diffraction of sintered undoped hydroxyapatite. J Am Ceram Soc 1997;80:37–44.

[159] Malina, Dagmara, Kamila Biernat, and Agnieszka Sobczak-Kupiec. “Studies on Sintering Process of Synthetic Hydroxyapatite.” *Acta Biochimica Polonica* 60, no. 4 (2013): 851–55.

[160] Zhou J, Zhang X, Chen J, Zeng S, De Groot K. High temperature characteristics of synthetic hydroxyapatite. J Mat Sci Mater Med 1993;4:83–5.

[161] Liao CJ, Lin FH, Chen KS, Sun JS. Thermal decomposition and reconstruction of hydroxyapatite in air atmosphere. Biomaterials 1999;20:1807–13.

[162] Cihlář, J., A. Buchal, and M. Trunec. "Kinetics of Thermal Decomposition of Hydroxyapatite Bioceramics." *Journal of Materials Science* 34, no. 24 (1999): 6121–31.

[163] Rahaman MN. Sintering of ceramics. Boca Raton: CRC Press; 2008.

[164] Bernache-Assollant D. Chimie-physique du frittage (Physico-chemistry of sintering). Paris: Hermes; 1993.

[165] Kreidler ER, Hummel FA. Phase relationship in the system SrO–P_2O_5 and the influence of water vapor on the formation of $Sr_4P_2O_9$. Inorg Chem 1967;6:884–91.

[166] Ryu HS, Youn HJ, Hong KS, Chang BS, Lee CK, Chung SS. An improvement in sintering property of b-TCP by addition of calcium pyrophosphate. Biomaterials 2002;23:909–14.

[167] Rabadjieva D, Tepavitcharova S, Gergulova R, Sezanova K, Titorenkova R, Petrov O, et al. Mg- and Zn-modified calcium phosphates prepared by biomimetic precipitation and subsequent treatment at high temperature. J Mater Sci Mater Med 2011;22:2187–96.

[168] Carbajal L, Caballero A, Sainz MA. Design and processing of ZnO doped tricalcium phosphate based materials: influence of b/a polymorph phase assemblage on microstructural evolution. J Eur Ceram Soc 2012;32:569–77.

[169] Ryu HS, Youn HJ, Hong KS, Chang BS, Lee CK, Chung SS. An improvement in sintering property of b-TCP by addition of calcium pyrophosphate. Biomaterials 2002;23:909–14.

[170] Asada M, Oukami K, Nakamura S, Takahashi K. Microstructure and mechanical properties on non-stoichiometric apatite ceramics and sinterability of raw powder. J Ceram Soc Jpn Int Ed 1988;96:583–6.

[171] Ryu HS, Hong KS, Lee JK, Kim DJ, Lee JH, Chang BS, et al. Magnesia-doped HA/ b-TCP ceramics and evaluation of their biocompatibility. Biomaterials 2004;25:393–401.

[172] Raynaud, S, E Champion, and D Bernache-Assollant. "Calcium Phosphate Apatites with Variable Ca/P Atomic Ratio II. Calcination and Sintering." *Biomaterials* 23, no. 4 (February 2002): 1073–80. doi:10.1016/S0142-9612(01)00219-8.

[173] Honeyman-Colvin, Paul, and Fred F. Lange. "Infiltration of Porous Alumina Bodies with Solution Precursors: Strengthening via Compositional Grading, Grain Size Control, and Transformation Toughening." *Journal of the American Ceramic Society* 79, no. 7 (July 1996): 1810–14. doi:10.1111/j.1151-2916.1996.tb07999.x.

[174] Glass, S. Jill, and David J. Green. "Permeability and Infiltration of Partially Sintered Ceramics." *Journal of the American Ceramic Society* 82, no. 10 (1999): 2745–52.

[175] Lin, Yung-Jen, and Yi-Chi Chen. “Cyclic Infiltration of Porous Zirconia Preforms with a Liquid Solution of Mullite Precursor.” *Journal of the American Ceramic Society* 84, no. 1 (January 2001): 71–78. doi:10.1111/j.1151-2916.2001.tb00610.x.

[176] Marple, Basil Richard, and David J. Green. “Graded Compositions and Microstructures by Infiltration Processing.” *Journal of Materials Science* 28, no. 17 (1993): 4637–43.

[177] Wang, Haibo, Jong-Kook Lee, Amr Moursi, and John J. Lannutti. “Ca/P Ratio Effects on the Degradation of Hydroxyapatite in Vitro.” *Journal of Biomedical Materials Research Part A* 67, no. 2 (2003): 599–608.

[178] Wang, Haibo, Jong-Kook Lee, Amr Moursi, and John J. Lannutti. “Ca/P Ratio Effects on the Degradation of Hydroxyapatite in Vitro.” *Journal of Biomedical Materials Research Part A* 67, no. 2 (2003): 599–608.

[179] Hoppe, Alexander, Nusret S. Güldal, and Aldo R. Boccaccini. “A Review of the Biological Response to Ionic Dissolution Products from Bioactive Glasses and Glass-Ceramics.” *Biomaterials* 32, no. 11 (April 2011): 2757–74. doi:10.1016/j.biomaterials.2011.01.004.

[180] David T. Scadden, ‘The stem-cell niche as an entity of action’, *NATURE*, 441 (7097):1075-9. (2006).

[181] Shinya Nakamura, M.S.,1 Takuya Matsumoto, D.D.S., Ph.D.,2 Jun-Ichi Sasaki, D.D.S.,2 et tl., ‘Effect of Calcium Ion Concentrations on Osteogenic Differentiation and Hematopoietic Stem Cell Niche-Related Protein Expression in Osteoblasts’ , *TISSUE ENGINEERING*: Part A, 16(8):2467-73 ,(2010)

[182] Ryu, Hyun-Seung, Hyuk-Joon Youn, Kug Sun Hong, Bong-Sun Chang, Choon-Ki Lee, and Sung-Soo Chung. “An Improvement in Sintering Property of B-Tricalcium Phosphate by Addition of Calcium Pyrophosphate.” *Biomaterials* 23, no. 3 (2002): 909–14.

[183] Carrodeguas, R.G., and S. De Aza. “A-Tricalcium Phosphate: Synthesis, Properties and Biomedical Applications.” *Acta Biomaterialia* 7, no. 10 (October 2011): 3536–46. doi:10.1016/j.actbio.2011.06.019.

[184] ohner M, Lemaitre J, Legrand AP, d’Espinose de la Caillerie JB, Belgrand P. Synthesis, X-ray diffraction and solid-state 31P magic angle spinning NMR study of a-tricalcium orthophosphate. J Mater Sci: Mater Med 1996;7:457–63.

[185] Carrodeguas, R.G., and S. De Aza. “A-Tricalcium Phosphate: Synthesis, Properties and Biomedical Applications.” *Acta Biomaterialia* 7, no. 10 (October 2011): 3536–46. doi:10.1016/j.actbio.2011.06.019.

[186] Combes, C., and C. Rey. "Amorphous Calcium Phosphates: Synthesis, Properties and Uses in Biomaterials." *Acta Biomaterialia* 6, no. 9 (September 2010): 3362–78. doi:10.1016/j.actbio.2010.02.017.

[187] Bohner M, Lemaitre J, Legrand AP, d'Espinose de la Caillerie JB, Belgrand P. Synthesis, X-ray diffraction and solid-state ^{31}P magic angle spinning NMR study of a-tricalcium orthophosphate. J Mater Sci: Mater Med 1996;7:457–63.

[188] Miranda, Pedro, Eduardo Saiz, Karol Gryn, and Antoni P. Tomsia. "Sintering and Robocasting of B-Tricalcium Phosphate Scaffolds for Orthopaedic Applications." *Acta Biomaterialia* 2, no. 4 (July 2006): 457–66. doi:10.1016/j.actbio.2006.02.004.